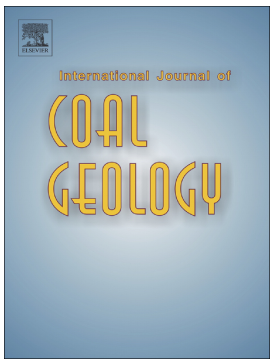

Cellular preservation and maceral development in lignite and wood from the Brassington Formation (Miocene), Derbyshire, UK

Jennifer M.K. O'Keefe, Matthew J. Pound, James B. Riding, Christopher H. Vane

PII: S0166-5162(20)30002-1

DOI: https://doi.org/10.1016/j.coal.2020.103452

Reference: COGEL 103452

To appear in: *International Journal of Coal Geology*

Received date: 1 January 2020

Revised date: 16 March 2020

Accepted date: 18 March 2020

Please cite this article as: J.M.K. O'Keefe, M.J. Pound, J.B. Riding, et al., Cellular preservation and maceral development in lignite and wood from the Brassington Formation (Miocene), Derbyshire, UK, *International Journal of Coal Geology* (2019), https://doi.org/10.1016/j.coal.2020.103452

Cellular preservation and maceral development in lignite and wood from the Brassington Formation (Miocene), Derbyshire, UK

Jennifer M.K. O'Keefe[1], Matthew J. Pound[2], James B. Riding[3], Christopher H. Vane[3]

[1]*Department of Physics, Earth Science, and Space Systems Engineering, Morehead State University, Morehead, KY 40351, USA,* [2]*Department of Geography and Environmental Science, Northumbria University, Newcastle upon Tyne NE1 8ST, UK,* [3]*British Geological Survey, Environmental Science Centre, Keyworth, Nottingham NG12 5GG, UK*

Abstract

Fossil wood is well known from the uppermost part of the Brassington Formation of Miocene age from two localities in Derbyshire, central England, UK, but its preservation has not been previously studied. Likewise, lignite is also present but has not been studied hitherto. This study examines preservation of selected wood samples using a combination of organic petrography and organic geochemistry. The best conserved exposure of the Kenslow Member of the Brassington Formation, representing the majority of the lower Kenslow Member, occurs at Bees Nest Pit. Disseminated woods occur throughout the Kenslow Member, with the greatest concentrations, and largest specimens, occurring around a meter below a thin lignite at Bees Nest Pit. The lignite is composed primarily of wood and charcoal, as well as organic-rich clay and leaves. Wood in the lignite and in the disseminated wood samples appear unaltered or charred in hand sample. Larger pieces typically have numerous cracks and pockets in the surface, highly suggestive of desiccation and white-rot prior to burial, but appear to be solid mummified wood overall. Drying in acetone and epoxy impregnation permitted the wood and lignite to be examined using reflected light microscopy, while air-dried wood samples were coated with gold-palladium and examined using SEM and prepared for organic geochemistry. All wood samples examined herein appear to be softwoods. Members of the "charred" group have high-reflecting exteriors and low-reflecting interiors in reflected white light illumination. Members of the "unaltered" group of tissues are consistently low-reflecting unaltered to slightly gelified textinite and ulminite A which display different reflectivity in transverse and radial sections. Random reflectance places the unaltered wood in the upper range of peat or lowest range of lignite B. Low-reflecting cells are primarily fiber cells and are strongly fluorescent. In most cases the three-ply fiber cell wall has begun to delaminate, a key feature of white-rot decomposition of the wood. Rays appear largely unaltered, and bordered pits show no evidence of fungal hyphae. Annual rings and vessels, by contrast, have undergone significant humification and have the appearance of ulminite and textinite, respectively. Near the wood margins, extensive pockets of rot show strong gelification, with the result that the cellular framework is gelified and brightly reflecting with isolated fibers present which still fluoresce. Huminite reflectance suggests that during very early

stage lignification, reflectance varies depending upon cellular orientation, with cells in transverse section being more highly reflective than those in radial section. Organic geochemistry indicates all the fossil woods are chemically altered relative to modern counterparts. The elemental ratios suggest these sit between modern wood and brown coal. The changes are probably due to loss of polysaccharide as compared to lignin structures. The spread in O/C and H/C is probably due to variable microbial alteration (e.g. white, soft or brown rot fungal decay), as also indicated by the organic petrography. This type of wood preservation is consistent with early coalification in aerial settings, and consistent with fungi recovered during palynological studies which are indicative of softwoods decaying in wet forest settings.

Keywords: Brassington Formation; coalification; fossil wood; Miocene; petrography; white-rot; UK

1. Introduction

Fossilized wood was recovered from the Kenslow Member of the Brassington Formation during fieldwork to support palynological studies at Lees Nest Pit, near Brassington, Derbyshire UK in 2013, 2017, and 2019 (Fig. 1). Upon initial examination, all of the wood specimens appeared intact. However, as they dried, it became apparent that the wood is highly fractured, with the light grey clay matrix of the Kenslow Member filling the cracks and much of the wood interiors, especially in the larger pieces. Regardless of this damage, the wood provides an important proxy for wetland dynamics during the latest middle Miocene (Serravalian) of the UK.

Miocene wood remains are known from many localities in the northern hemisphere, including Canada, China, the Czech Republic, Germany, Hungary, and Turkey (Hoffmann and Blanchette, 1997; Figueiral et al., 1999; Erdei et al., 2009; Hámor-Vidó et al., 2010; Cheng et al., 2014, 2018; Bardet and Pournou, 2015; Acarca Bayam et al., 2018; Mustoe, 2018; Mantzouka et al., 2019). Both angiosperm and gymnosperm woods have been reported, although in many cases gymnospermous woods dominate the assemblages, especially in and above coal seams (Hoffmann and Blanchette, 1997; Figueiral et al., 1999; Erdei et al., 2009; Hámor-Vidó et al., 2010. Many examples of Miocene wood occur as mummifications, rather than as coalifications or silicifications (Mustoe, 2018). Mummifications are an interesting and somewhat unusual preservation state, whereby the wood is largely unaltered, even after millions of years of burial. In cases reported from Germany, mummified wood samples are prone to cracking along the

annual rings upon drying (Hoffmann and Blanchette, 1997). In Hungary, woods display yellow to reddish-brown color, reminiscent of modern wood, and intense epifluorescence, which is light blue in UV excitation for extremely unaltered tissue of cellulose-rich wood (Hámor-Vidó et al. 2010).

Fossil wood was first reported from the Kenslow Member by Yorke (1954, 1961). Boulter (1969), Boulter and Chaloner (1970) and Boulter (1971), identified four gymnospermous taxa, but did not provide any photographic evidence or wood descriptions to support the identifications of *Abies* (fir), *Pinus* (pine), *Picea* (spruce) and Taxodiaceae (they suspected *Cryptomeria* or *Sciadopities* in the bald cypress family). Logan and Thomas (1987) examined lignin derivatives in fossil "Taxodiaceous" wood from Bees Nest Pit. They found that lignin from these wood samples has undergone significant demethoxylation and some destruction of phenolic aldehydes. They suggest that white-rot fungi had caused significant degradation of woody tissues. Decomposed fossil wood can be difficult to identify, as has been demonstrated (van den Burgh, 1973; Blanchette et al., 1991; Figueiral et al., 1999), and classification tends to base upon a few specific characters, especially when determining if wood is angiospermous or gymnospermous. These characters may or may not be visible in either thin-sections or polished sections, depending upon the compaction state and degradation state of the wood. While some authors advocate charring of samples prior to attempts at identification as a means of making wood characters more visible (Figueiral et al., 1999), most researchers impregnate mummified woods with epoxy (Abad, 1988, Hámor-Vidó et al., 2010) or polyethylene glycol (Hoffmann and Blanchette, 1997); or simply wet and slice it prior to mounting in glycerin jelly (Blanchette et al., 1991; Wang et al., 2017, Mantzouka et al., 2019). These latter options have the advantage of conserving the preservational state of the wood such that characteristic damage patterns caused by bacteria, fungi, and chemical alteration can be observed (Blanchette et al., 1991a,b; Hoffmann and Blanchette, 1997).

Here we report on the preservation state of selected wood samples recovered during fieldwork at Bees Nest Pit, suggest wood affinity based on taxonomic features preserved in the samples and visible in reflected light petrography and SEM, and comment upon the decomposition features. Together, wood identification features and damage patterns allow us to add to the growing body of knowledge about the paleoecology and depositional settings of the Kenslow Member at this important locality.

2. Geological background and setting

The Brassington Formation is the most extensive onshore Miocene succession in the UK. It is a fining-upwards sequence of sands, gravels, pebble beds, clays and, occasionally, a wood bearing lignite which have suffosed into karstic hollows in the Peak District of Derbyshire and Staffordshire, UK (Walsh et al., 2018). The formation is subdivided into three members; these are the Kirkham, Bees Nest and Kenslow members in ascending stratigraphic order (Boulter et al., 1971). The lowermost Kirkham Member is up to ~60 m of sand, gravel and pebble beds believed to be the weathering products of Triassic sandstones to the south. It is envisaged as an alluvial/fluvial sheet sand extending northwards across the present-day Peak District (Walsh et al. 1972). The overlying Bees Nest and Kenslow members are relatively thin, clay-rich units assumed to be lacustrine deposits which accumulated on the subjacent Kirkham Member. The three members of the Brassington Formation suffosed into large karst cavities during the Pliocene (Walsh et al. 2018, fig. 12).

Only the Kenslow Member is fossiliferous, and this unit contains biostratigraphically significant pollen and spores (Pound et al., 2012a; Pound and Riding, 2016). The Kenslow Member is considered to represent different parts of the Miocene in the two disused quarries that have been studied. In Bees Nest Pit it is Serravallian (13.65–11.61 Ma), whereas the Kenslow Member at Kenslow Top Pit is Tortonian (11.61–7.25 Ma) in age (Pound et al., 2012a; Pound and Riding, 2016). By contrast, there are no biostratigraphical data from the underlying Kirkham and Bees Nest members.

3. Materials and methods

The fossil wood and the lignite studied herein are all from Bees Nest Pit (53.09°N, 1.64°W) near the village of Brassington (Fig. 1). Samples were collected in 2013, 2017, and 2019 from the uppermost Kenslow Member; this is a ~2 m bed of massive grey clay with a ~30 cm thick lignite lentil near the top (Figure 2; Table 1). All the disseminated wood samples are from within the grey clay in the middle of the Kenslow Member as exposed at Bees Nest Pit, and oriented

column (pillar) samples of the lignite bed were collected from the uppermost part of the unit. Based on palynology, the material is considered to be Serravallian in age (Pound and Riding, 2016).

Fossil wood sample NU13-001 and charcoal samples NU13-002 and NU13-003 were dried in ambient conditions, sectioned using a razor blade, mounted on carbon film and sputter-coated with gold-palladium for SEM imaging on a MIRA3 Tescan at 20 kv at Northumbria University.

The disseminated fossil wood taken to Morehead State University (JOMSUGL 908, JOSMUGL 909, and JOMSUGL 910) was dried in a series of acetone baths and impregnated with Pace Metallographic Low Viscosity ULTRATHIN® Epoxy prior to sectioning (López-Buendía, 1998; Frank and Bend, 2004). Radial, tangential, and longitudinal sections were made of each wood fragment using oil- and water-cooled cut-off saws, as appropriate for the size of the specimen.

Lignite column samples (JOMSUGL 1245 and JOMSUGL 1246) were dried in an 80°C oven for 12 hours. This temperature was used to prevent modern fungal growth during drying. After drying, the exterior 1-2 cm of the original column was removed to minimize heating effects on sample reflectances. The remaining central portion was placed in silicone block molds, and epoxy impregnated using the methods of Jewell (2004) and O'Keefe (2008). The analyzed surfaces of both wood and lignite samples were polished to a 0.05 µm finish using alumina on a silk cloth following ASTM D5671 - 95(2019). All samples were analyzed on Leitz Ortholux Pol II reflected light microscope equipped with halogen white light illumination and Cool LED blue light illumination at 440 nm with a K515 filter. Photomicrographs were captured using a Leica MC170 camera and LAS® software. Maceral analysis were completed for the lignite samples; these followed ICCP System 1994 terminology (ICCP, 2001; Sýkorová et al., 2005; Pickel et. al., 2017) and the counting methods of O'Keefe (2008) for oriented-block studies of lignite.

Reflectance measurements were completed using a Leitz MVP photomultiplier with analog display on a Leitz Ortholux with 100-watt quartz halogen white light illumination and 500x magnification using an oil immersion objective. A glass reflectance standard with reflectance of 0.299 was used to calibrate the photomulitplier. Results were cross-checked using the grey-scale

method applied to photomicrographs. To generate the calibrated curve for the grey-scale method, a set of six glass standards with certified reflectances of 0.299, 0.506, 0.94, 1.025, 1.381, and 1.672, manufactured by J. Cole of Pennsylvania, were photographed under the same conditions as noted above for the macerals. Greyscale measurements of photographs of each glass standard were plotted against their respective calibrated values to produce the curve. A new curve was generated each time the microscope bulb and image capture system are turned on to account for variations in illumination. The equation for this curve was then used to calculate random reflectance. A 5-micron square measuring spot was used in the Leitz MVP photomultiplier. A minimum of 50 and maximum of 100 spots per sample were measured with the photomultiplier. A 2-micron circular spot was used for greyscale measurements. Five spots, distributed as the corners and center point of a box, were measured on each of 20 maceral photographs obtained per sample, for a total of 100 measurements per sample. Wood xylotomy features were identified using Richter et al. (2004), and compared with published works on Miocene fossil wood, including Obst et al. (1991), Blanchette et al. 1991), Figueiral et al. (1999), Erdei et al. (2009), Bardet and Pournou (2014), Wang et al. (2017).

Organic geochemical measurements were undertaken on eight discrete fossil woods (OG7, OG10a, OG10b, OG11, OG13, OG21, OG100, OG101) from the grey clay of the Kenslow Member. All outer surfaces were cleaned of sediment using a wire brush, washed with deionised 18Ω water and oven dried at 40°C for 24 h. Wood powders were collected using a drill (Dremel 400) fitted with a diamond bit. Samples were transferred to 10 ml glass vials, freeze dried and ground to pass a 63µm mesh sieve using an agate pestle and mortar. Non-structural compounds were removed by sequential solvent extraction with 2 × 8 ml MeOH and 3 × 8 ml DCM by sonication 12 min (Camlab, Transonic T470H, 300 W). The organic carbon, hydrogen and nitrogen content of each wood was determined (n=8), using a Carlo Erba 1106 elemental analyzer. Oxygen content was estimated by difference and ash content was determined gravimetrically following combustion of the dry powdered wood at 650 °C for 18 h (Vane et al., 2003).

4. Results

4.1. Scanning Electron Microscopy (SEM)

SEM imaging of sections from NU13-001 revealed that much of the apparently macroscopically "unaltered" wood, was actually substantially changed under higher magnification (Fig. 3). Most of the cells have collapsed, and, at high magnification, the wood appears quite homogenous (Fig. 3c; NU13-001). This aspect is consistent with the appearance of ulminite in reflected light microscope. Transverse sections of slightly charred wood (Figs. 3d–f) exhibit growth rings, but even here, it was not possible to image sufficient cellular features to produce a firm identification of the wood. Given the regularity of the pits, shape of the cells, we suspect conifer wood (perhaps *Pinus* or *Cryptomeria* or *Taxodium*), however hardwood members of the Fagales (*Fagus* or *Quercus*) impacted by white-rot can have a similar aspect. Charcoal fragments (NU13-002 and NU13-003) collected in 2013 (Figs. 3g–i) all appear to be radial to tangential sections of conifer wood. Again, insufficient diagnostic characters to assign it to a specific type were present.

4.2. The thermal maturity of the fossil wood

Disseminated wood samples JOMSUGL 908, JOMSUGL 909, and JOMSUGL 910 from the middle part the Kenslow Member, and one column (pillar) sample from the lignite lentil in the upper part of the Kenslow Member as exposed at Bees Nest Pit have been examined to date. Random reflectance measurements were taken from transverse sections of all the disseminated wood, and from transverse and longitudinal radial sections of sample JOMSUGL 908. Random reflectance measurements of wood contained in the lignite bed were made on polished surfaces in the oriented blocks, thus represent reflectance of materials facing to the southwest.

Upon examining the samples, it became clear that our macroscopic designation of "charred" and "not charred" was over-simplistic (Fig. 4; Table 2). The exterior of wood fragment JOSMUGL 908 in longitudinal section contains brighter-than-expected, collapsed cellular material with a random reflectance of 0.98%, consistent with inertinite, filling small pockets between low reflecting wood fibers (0.204%), with exceptionally swollen rectangular cells, consistent with textinite (Fig. 4a). A narrow transition zone, less than 2 mm wide, has a random reflectance of 0.528%; this narrow transition zone parallels the trend of the exterior surface of the wood but can

extend several millimeters into the wood, primarily along the tracheids (Fig. 4b). In longitudinal radial section, the transition zone is not visible, and the collapsed and swollen wood remains display a much lower reflectance, 0.14%. This suggests variability in reflectance depending upon wood cell orientation, which will be explored further in a future study. Wood sample JOMSUGL 909, which was designated as charred, contained no visibly charred material, and indeed, displayed a uniform random reflectance of 0.103% throughout. Wood sample 910 displayed a uniform random reflectance of 0.31% throughout. Huminite reflectance was measured on woody bands in the lignite. In the second decimeter from the top of the seam (1245-2), uncharred wood displayed a random reflectance of 0.21%, while charred wood displayed a random reflectance of 2.86%. Within the third decimeter from the top of the seam (1246-1) uncharred wood displayed a random reflectance of 0.21%. In all cases, uncharred wood and lignite have huminite reflectances that fall into the peat to Lignite B categories.

4.3. Macerals and wood preservation

Wood preservation is highly variable, with somewhat altered xylite to early-stage textinite, both having bright yellow epifluorescence, to clearly decayed textinite, with reduced orange fluorescence, to gelified non fluorescing ulminite. Here we discuss maceral evidence for wood preservation.

4.3.1. Samples 908, 909, and 910

Sample 908 was sectioned in three orientations: tangential, radial, and transverse. Samples 909 and 910 were only available as transverse sections. In transverse section along the margin of the wood fragments, dark cells, corresponding to textinite A, (Fig. 4a) are directly adjacent to fusinite bogens. This brightly reflecting material extends approximately 1 mm into the body of the wood (Figs. 4d,e), and is coupled with dimly fluorescing fiber cells that display some evidence of white-rot decay, including cracking and delamination of the three-ply cell wall (Fig. 4f).

The variability in preservation around the margins of each of the wood samples is extremely interesting. Characteristic selective decay and gelification structures can be readily seen in fluorescent light (Fig. 5a). In some places along the margins of the wood, cell walls have collapsed. In extreme cases, these have reduced fluorescence where loss of cellulose, in addition

to lignin, is likely high, as suggested by organic geochemical results, below, resulting in greying and early-stage conversion to huminite macerals visible in white light (Fig. 5b). In other places, the wall is relatively swollen and extremely degraded to the point of being jumbled and broken, but still contain enough cellulose to fluoresce well and remain red-brown in white light (Figs. 5c,d). In tangential section, dark cells, which with no prior knowledge of wood structure would probably be counted as ulminite B. The side view of the dark cells counted as textinite A in transverse section. The tracheids, which are not readily apparent in transverse section, appear as much brighter ulminite B, verging on semifusinite, given their reflectance relative to the mean random reflectance (Fig. 4b; Table 2). The radial section from the interior of the wood fragment was remarkable, in that the wood appeared largely unaltered (Fig. 4c). Here the scleriform pits can clearly be seen, and the wood does not appear to have been gelified. Funginite occurs as fungal sclerotia in the remnant clay encasing the wood fragment, however (Figs. 6a,b), no evidence of fungal hyphae were seen in any portions of the fragment. Sporinite and cutinite (Figs. 6c–e), also, occur as disseminated remains within the clay matrix.

4.2.2. Lignite bed samples

A total thickness of 30.6 cm of organic matter rich clay and lignite from the western side of the lignite exposure were collected as oriented column (pillar) samples and analyzed herein (Figs. 7−9; Table 3). The lowermost sediment from 30.6 cm to 28.8 cm is a dark grey silty clay with minor huminite and abundant (15-25%) sporinite macerals. Huminite (Figs. 9a–d) appears to be primarily as telohuminite, the majority of which is textinite in the lower half of the column and ulminite in the upper half, although in mineral matter-rich horizons detrohuminite is most common (Table 3, Figs. 7, 8). Above this point, pyrite is present and reaches countable levels at 10.8 cm depth. Liptinite (Figs. 9g–h) is dominated by suberinite, except at 10.8 cm and 23.4 cm, where cutinite is dominant. Sporinite is never more than 2.4% of the total. Liptodetrinite does not occur. Inertinite (Figs 9e–f) is generally rare, never reaching more than a few percent. Where higher, inertinite is primarily semifusinite; inertodetrinite does not occur.

Four distinctive woody bands occur in the lignite bed. These are: 27.9 cm–26.1 cm; 19.8 cm–18.9 cm; 17.1 cm–11.7 cm; and 9.0 cm–7.2 cm. Each band appears to be composed of a single piece of wood, each of which is primarily huminite with minor inertinite (semifusinite) and liptinite (suberinite). Regardless of the macroscopic appearance of the wood fragments, no piece

is entirely pyrolised. Each of the wood samples encountered has slightly different apparent preservation, in part because of variations in orientation, highlighted by the study of sample 908, above. Wood in the lowermost and third from the bottom bands are oriented as transverse sections (Figs. 9a–b). Wood in the second from the bottom band is oriented as a tangential section (Figs. 9c–d). It is not possible to determine the orientation of the wood in the uppermost band, as it is both more gelified than other examples, and also the only band that contains obvious funginite in the huminite (Fig. 9e). Of note, euhedral pyrite occurs disseminated within this more gelified band (Table 3). Euhedral pyrite is indicative of sufficient iron presence to permit methanogenic bacteria to enhance gelification.

4.4. Wood morphology and xylotomy

The disseminated wood samples in both the loose pieces and those within the lignite bed exhibit square cells in radial section. This cell shape is more common in gymnospermous wood than angiospermous wood. Growth rings are clearly visible in the SEMs of sample NU13-001, but fall into the International Association of Wood Anatomists (IAWA) classification of "indistinct," in that there is no clear difference between earlywood and latewood (Figs. 3d,e; Richter et al., 2004). The growth rings are very narrow, typically 5 cells (Figs. 3d,e), indicative of slow radial growth of the tree, make it very difficult to determine the nature of the transition between the rings (Richter et al., 2004). In SEM (Figs 3f,h), reflected white light (Fig. 4c) and epifluorescence (Figs. 10a–d,g,h), the wood appears predominantly uniseriate in radial sections, that is, the tracheid pits are organized mostly in a single column within the cell. A second tracheid pit or second row of tracheid pits may be present (Figs 10a–d); where present, these pits are parallel to the other row. Wall thickness is not diagnostic for the charcoalified samples, such as portions of NU13-001, but can be useful in the mummified samples. In all cases examined to date, the wood fragments disseminated in the Kenslow Member have thick walls (Figs. 4a,d–f). The cell walls of the ray tracheids are smooth, with a Hudson scale of 1–2 (Hudson, 1960) (Figs. 10e,f). In some orientations, a pattern of two latewood cells between tracheids is observed (Fig. 4b). Infrequently, cupressoid-taxodioid cross-field pits (shaped like the capital letter O) are visible (Fig. 10g).

4.5 Bulk Elemental Organic Geochemistry

Total organic carbon (TOC) of woods of the Kenslow Member ranged from 60.5 to 38.3 % with a mean of 54.8 %, oxygen content ranged from 30.6 to >40 %, and hydrogen ranged from 6.1 to 3.4 %, whereas nitrogen content ranged from 0.1 to 1.1 % (Table 4). The ash contents varied across the eight samples from as low as 0.7 to 37.6 % with a mean of 9.8 %. Chemical characterization of fossil woods and underlying alteration processes such as microbial decay and pressure/temperature maybe visualized using a van Krevelen bi-polot which summarizes main elemental composition as ratios (Fig. 11). Comparison of Kenslow Member woods (atomic O/C ratios of 0.5 and atomic H/C of 1.2) with modern wood, lignites and more thermally mature coals show that the woods from the Kenslow Member plot precisely between modern wood and low rank coals (Fig. 11). In modern woods polysaccharides have an atomic O/C of 0.8 and H/C of 1.7 whereas more aromatic lignin bioploymer has an atomic O/C of 0.3 and atomic H/C of 1.2. Owing to the greater proportion of polysaccharides to lignin, unaltered modern woods have atomic O/C ranging from 0.7 to 0.9 and atomic H/C of 1.5 to 1.8 (Fig. 11).

In the current study, the Kenslow Member fossil woods all plot outside the ranges expected for modern woods, confirming that the sediments and selected samples analyzed were not contaminated by modern vegetation/rootlets. From a biochemical standpoint, the most plausible explanation for the lower values in the Kenslow Member samples as compared to modern wood counterparts is that the woods have preferentially lost polysaccharides relative to lignin. The position of the Kenslow Member woods across the wood coalification continuum and the clear general downward trajectory to lower atomic O/C and H/C similar to purified lignin is most likely explained by a combination of biotic (fungal and bacterial) and possibly abiotic reactions which alter the relative proportion of polysaccharides to other bioploymers as well as alteration of lignin by a variety of reactions including dehydroxylation alkyl side chains, cleavage of β-O-4 bonds and demethoxylation (Hatcher and Clifford, 1997; Vane and Abbott, 1999; Vane et al., 2001a,b). White-rot fungal decay modifies woody tissues by the oxidative decay of lignin such that lignin is preferentially decomposed relative to polysaccharides and that remaining residual lignin structure contains a greater amount of carboxyl acid structures (COOH) on lignin side chains (Vane et al., 2006; Vane et al., 2003b; Vane et al., 2001a,b,). Conversely, brown-rot decay mainly decompose polysaccharides whereas soft-rot decay may preferentially decompose other biopolymers such as tannins and lignins (Vane et al., 2005). Therefore, it is plausible that

the spread of atomic O/C values encountered in the Kenslow Member woods is at least in part influenced by variable fungal decomposition including putative white rot fungal degradation.

5. Discussion

Disseminated woods occur in the Kenslow Member between a basal woodground and a lignite bed. The preservation of the wood ranges from nearly unaltered to early-stage coalification, producing an array of xylites and early-stage huminite macerals primarily textinite and corpohuminites. In transverse and radial sections, many distinctive wood characters are still present. From these, additional information about climate at the time of deposition and wood types can be garnered.

The presence of indistinct growth rings in all of the disseminated wood samples, whether viewed in reflected light or through SEM, suggests that growth occurred in a warm setting, perhaps tropical or subtropical (Richter et al., 2004). Paleoclimate reconstructions from the Kenslow Member, based on pollen and spores, also indicate a subtropical wet climate (Pound and Riding, 2016). Furthermore, that the specimens collected represent parts of young trees, branches and/or those that experienced slow radial growth, as the rings only average five cells. This growth pattern is not unusual in tropical plantation-grown members of the Pinaceae (Richter et al., 2004). Uniseriate pitting, with periodic double rows of pits that are parallel, rather than offset, is also common in the Pinaceae. Thick walls, visible in the fiber cells, as well as smooth ray tracheid walls, are also features of some Pinaceae, and in the case of the smooth walls, point toward the *Strobus* section of pines (Richter et al., 2004). The pattern of two latewood cells between tracheids is common in taxodiaceous trees (Richter et al., 2004), but also known to occur in pines (Wang et al., 2017). Cupressoid-Taxodioid cross-field pits are also diagnostic of members of the Cupressaceae and taxa formerly assigned to the Taxodiaceae (Richter et al., 2004), however, compression can warp pits, thus this character must be used with caution. Additionally, cupressoid-taxodioid pitting has been reported in Miocene pines (Wang et al., 2017). Taken together, the characters suggest that the material studied are members of the

Pinaceae, likely a member of the section *Parrya*, such as *P. krempfii* or *P. aristata* (van der Burgh, 1973; Ickert-Bond, 2001; Wang et al., 2017), however, assignation to the Cupressaceae, based on cell wall thickness and pitting type, cannot be entirely ruled out (Hoffmann and Blanchette, 1997; Figueiral et al., 1999; Jeong et al., 2012). Abundant and diverse gymnosperm pollen has been recovered from the Kenslow Member at Bees Nest Pit and does not aid wood identification (Boulter, 1971; Pound and Riding, 2016).

The wood preservational style and disseminated nature in the Kenslow Member suggests transported, rather than *in-situ* remains, however, given the lack of inertodetrinite and liptodetrinite macerals, the distance of transport was likely relatively short. Some of the trees were undoubtedly burned prior to burial, with remnant charcoal present on the outermost surface of sample 908, fragments NU13-002 and NU13-003, and brighter-than expected reflectance extending a millimeter or more into the surface of many pieces. This brighter than expected horizon, which does not quite attain semifusinitic-levels of reflectance, coupled with the blackened color of the wood samples, many of which were originally classified as "charred" in hand sample, is likely reflective of a pyrolysis front produced during wood combustion (Hudspith and Belcher, 2020). Here the outer charcoalified layer, represented by fusinite, was likely removed during transport, leaving the thermally altered, but not charcoalified, layer behind.

Other evidence observed in the wood samples is suggestive of fungal decomposition prior to incorporation into the Kenslow Member clay. The separated and variably fluorescing cells in Fig. 5 are a result of loss of the middle lamella through white-rot (Blanchette, 1984, 1991, 2000), which is progressively worse from Fig. 5a through Figs. 5c–d. In thick-walled cells (Figs. 3d–f), this evidence for white-rot includes cracking and delamination of the three-ply wall (Fig. 3f), while the separation of cells and destruction of surrounding material (Figs. 4d–e) is an extreme case of white-rot decay. Given the bright, apparently gelified macerals surrounding the rotted tissues (Figs. 4d–e), it is likely that the trees were diseased prior to a wildfire event.

Previous palynological study of the Kenslow Member (Pound et al., 2012a; Pound and Riding, 2016) has shown that pine pollen is dominant (28%), while pollen of Cupressaceae are relatively uncommon (4.68%). While pine pollen is known for "flooding" samples and obscuring the signal

of locally important plants, the assemblage at Bees Nest Pit has been described as representing a subtropical, wet coniferous forest (Pound and Riding, 2016). The Serravalian has been proposed as having relatively drier conditions than the "washhouse climate" of the Late Miocene in Europe (Böhme, 2004; Böhme et al., 2008; Pound et al., 2012b). It has been proposed that this change in the regional hydrological regime was due to a switch from a Serravallian trade-wind (northeast to southwest) dominated circulation to a Late Miocene atmospheric circulation dominated by, the more modern, westerlies (west to east) (Quan et al., 2014). During the Miocene, the UK formed a peninsula of northwest Europe projecting into the North Atlantic and whether the Serravallian trade-wind dominated atmospheric circulation had any influence on the local precipitation regime is unknown, but a modest increase in precipitation has been reconstructed from the Netherlands from the Serravallian into the Tortonian (Donders et al., 2009). Whereas paleoclimate reconstructions from the Kenslow Member indicate a modest reduction in mean annual precipitation from the Serravallian into the Tortonian (Pound and Riding, 2016). Further complexity is introduced by regional paleobotanical data indicating the presence of a modern-like Gulf Stream from 15 Ma that would have brought heat and moisture into western Europe (Denk et al., 2013). Given the presence of charcoal it is possible that, like today, cyclical droughts may have impacted the region, increasing the likelihood of wildfires.

Indeed, cyclical drought may have been a causative agent of peatland establishment during the deposition of the uppermost part of the Kenslow Member at Bees Nest Pit. Research in North America has shown that drought events can lower water levels in lake systems to the point that peatland plants can colonize the shallow-water or exposed, moist substrate (Ireland and Booth, 2011; Ireland et al., 2012, 2013, Booth et al., 2016). Once colonized, rising water levels coeval with an end to drought conditions can lead to the development of floating peat mats and continued *in-situ* peat development. Like the Quaternary and Holocene North American peats, the lignite studied from Bees Nest Pit, and also recorded at the nearby Kenslow Top Pit (Pound et al., 2012a, Pound and Riding 2016) are thin, and overlie sediments interpreted as lacustrine. At Bees Nest Pit, the "lignite" begins as several centimeters of silty organic-rich mudstone, equivalent to clayey-detrital gyttja, and returns to this state between the woody horizons. This suggests periods of drier conditions followed by a rising water table resulting in formation of a floating bog in the mire with anaerobic decomposition of the original peat matrix occuring below this floating material. The presence of fusinite with sub-centimeter-scale distributions is

suggestive of either combustion of emergent vegetation (Korasidis et al., 2016), or incorporation of charcoal from upland wildfires (possibly the source of charred woods) into the peat during flooding and siliciclastic sedimentation events following drought intervals (Scott, 2018). In the Kenslow Member, small-scale fusinite and semifusinite pieces occur periodically through the lignite. The majority of these particles occur in association with or just following siliciclastic influxes (Figure 7). In this sense, the lignites capping the Kenslow Member at Bees Nest Pit, and the lignite capping the same unit at nearby Kenslow Top Pit, while younger, serve to highlight increasing climate variability in the upper section of Middle and Late Miocene. An interpretation supported by reconstructed seasonal precipitation from the Kenslow Member that shows a shift from nearly year-round wet to a more winter-wet hydrological regime (Pound and Riding, 2016).

Inertinite macerals record wildfire intensity (MacParland et al., 2009), and as such, are useful indicators of the types of wildfire that contributed charcoal to the Kenslow Member clays. The inertinitic material measured in disseminated wood pieces is likely erosional remnants of the pyrolysis front, not actual surface charcoal, thus not useful for this exercise. The inertinite recovered in the lignite, however, have a mean random reflectance of 2.87%, indicative of a 1–5 hour charring temperature between 550 and 650°C (MacParland et al., 2009). This temperature range is suggestive of a short-lived crown fire or a smouldering ground fire (Scott, 2009, 2018). The high standard deviation of these measurements (Table 2) suggests that the fragment preserved in the lignite experienced differential thermal alteration from the exterior to the interior of the sample (Hudspith and Belcher, 2019; MacParland et al., 2009).

The depth of burial of the Kenslow Member has been a source of curiosity for many years, as no overlying sediments remain post-glaciation. Huminite reflectance data suggests that wood reflectance was suppressed below the lignite, quite possibly due to variations in the thermal conductivity of the materials, lignite being more thermally conductive than the Kenslow Member clays (Mukhopadhyay, 1994), equally possibly due to variations in the coalification process and orientation of the macerals used for reflectance measurements, as noted above. The impact of early-stage lignification on rank is not well understood, however, in situations such as the Brassington Formation, lignite rank can provide some clues. The most deeply buried huminite macerals from the lignite had a mean random reflectance of 0.29%, indicating a rank of Lignite B. This can imply million-year burial at 60°C (Gallagher, 2012), or shorter burial at higher

temperature. The modern geothermal gradient is rather complex in the southern Pennines, with unexpected highs and lows within very short distances due to the highly fractured and karstified limestone in the region, which act as conduits for hydrothermal fluids feeding mineral and hot springs. At 1000 m depth, measured temperatures range from 42–54°C; thus, a maximum burial depth of slightly more than 1000 m for a short time period is possible, however, shallower burial for a long time period is more likely, especially given the varying degrees of lignificaiton indicated by the disseminated wood through both organic geochemistry (Figure 11) and organic petrography.

6. Conclusions

This is the first study of wood and lignite recovered from the Kenslow Member of the Brassington Formation from Bees Nest Pit, Derbyshire. Wood samples display variable huminite reflectance depending on the gelification-humification degree of disseminated woods and lignite, consistent with peat and are preserved primarily as mummifications. Some mummifications of disseminated wood have singed surfaces, suggesting they may have been washed into the sinkhole lake following fire events. Most samples contain decomposition patterns consistent with white-rot decay. The disseminated wood samples examined during this study are remarkably similar and are likely members of the *Strobus*-section of the pines (Pinaceae), although some characters suggest they may be members of the Cupressaceae. Additional study is needed to firmly assign the samples to either the Pinaceae or the Cupressaceae. Wood features confirm deposition in a subtropical wet climate, as previously suggested by Pound et al. (2016, 2019). Periodic drought conditions are suggested by the presence of charred wood in the Kenslow Member underlying the lignite, and by the lignite itself (Booth et al., 2016). Charcoal from within the lignite is suggestive of episodic smoldering ground fires or distant crown fires. Clastic influx into the mire may have been in part driven by increased runoff following fires.

Elemental (C, H, N, O) geochemistry shows the fossil woods are chemically between modern wood and brown coal, this is most likely due to relative loss of polysaccharides as compared to lignin. Given that the woods were all collected from the same unit the spread in key ratios is not

likely to be caused by thermal/pressure effects but may instead be attributed to variations in the extent and type of fungal decay, or possibly variations in transport distance or highly localized variations in water table depth and associated extent of aerobic decay.

Reflectance measurement of low reflectivity textinite highlights the variability in reflectance depending upon wood cell orientation. This contributes to the larger standard deviation which may be seen in reflectance measurements of very low rank coals. The lignite attained a random reflectance of 0.29% and reached the rank of lignite B; disseminated woods below the lignite have variable reflectance depending upon degree of lignification as determined by organic petrography and organic geochemistry. This suggests a maximum burial depth of approximately 1000 m; given the modern regional geothermal gradient and wood preservation states, likely less.

Results of petrographic and geochemical study are consistent with previous palynological indications that the Kenslow Member was deposited in a flooded mire or lacustrine setting surrounded by pine woodlands. Peat accumulation was likely initiated following a localized drought, and the presence of alternating bands of clay-rich and wood-rich coal suggests periodic drought conditions during peat development. Peat production likely terminated following a flooding event which produced the paler clay capping the deposit.

Acknowledgements

This research was facilitated by a William George Fearnsides Fund Grant (2013) and an Elspeth Matthews Fund Grant (2019) awarded to MJP by the Geological Society of London. We are grateful to Jayne Spencer, the owner of Bees Nest Pit and Natural England for facilitating access to this disused quarry. Lesley Dunlop, Peter Jones, Michael Lim and Cameron Reaveley are thanked for their help with the fieldwork. Pietro Maiello is thanked for providing support on the SEM, including sputter coating the samples. James C. Hower is thanked for use of polishing equipment at the University of Kentucky Center for Applied Research. James B. Riding and Christopher H. Vane publish with the approval of the Executive Director, British Geological Survey (UKRI). This manuscript was substantially improved by suggestions from our reviewers, David Dilcher and Mariá Hámor-Vidó.

References

Acarca Bayam, N.N., Akkemik, Ü., Poole, I., Akarsu, F., 2018. Further contributions to the early Miocene forest vegetation of the Galatin Volcanic Province, Turkey. Palaeontologia Electronica 21.3.40A, 1–42. https://doi.org/10.26879/816.

Bardet, M., Pournou, A., 2015. Fossil wood from the Miocene and Oligocene epoch: chemistry and morphology. Magnetic Resonance Chemistry 53, 9–14.

Blanchette, R.A, Cease, K.R., Abad, A.R., Burnes, T.A., Obst, J.R., 1991a. Ultrastructural characterization of wood from Tertiary fossil forests in the Canadian Arctic. Canadian Journal of Botany 69, 360–368.

Blanchette, R.A., Cease, K.R., Abad, A.R., Koestler, R.J., Simpson, E., Sams, G.K., 1991b. An evaluation of different forms of deterioration found in archaeological wood. International Biodeterioration 28, 3–22.

Blanchette, R.A., 1984. Screening wood decayed by white rot fungi for preferential lignin degradation. Applied and Environmental Microbiology 48, 647–653.

Blanchette, R.A., 1991. Delignification by wood-decay fungi. Annual Review of Phytopathology 29, 381–398.

Blanchette, R.A., 2000. A review of microbial deterioration found in archaeological wood from different environments. International Biodeterioration & Biodegradation 46, 189–204.

Böhme, M., 2004. Migration history of air-breathing fishes reveals Neogene atmospheric circulation patterns. Geology 32, 393–396.

Böhme, M., Ilg, A., Winklhofer, M., 2008. Late Miocene 'washhouse' climate in Europe. Earth and Planetary Science Letters 275, 393–401.

Booth, R.K., Ireland, A.W., LeBoeuf, K., Hessl, A., 2016. Late Holocene climate-induced forest transformation and peatland establishment in the central Appalachians. Quaternary Research 85, 204–210.

Boulter, M.C., 1969. Cryptomeria– a significant component of the European Tertiary. Paläontologische Abhandlungen B 3, 279–287.

Boulter, M.C., 1971. A survey of the Neogene flora from two Derbyshire pocket deposits. The Mercian Geologist 4, 45–61.

Boulter, M.C., Chaloner, W.G., 1970. Neogene fossil plants from Derbyshire (England). Review of Palaeobotany and Palynology 10, 61–78.

Boulter, M.C., Ford, T.D., Ijtaba, M., Walsh, P.T., 1971. Brassington Formation: A newly recognised Tertiary Formation in the Southern Pennines. Nature Physical Science 231, 134–136.

Cheng, Y.-M., Wang, Y.-F., Liu, F.-X., Jin, Y.-G., Mehrotra, R.C., Jiang, X.-M., Li, C.-S., 2018. The Neogene wood flora of Yuanmou, Yunnan, southwest China. LAWA Journal 39, 427–474.

Cheng, Y.-M., Wang, Y.-F., Li, C.-S., 2014. Late Miocene wood flora associated with the Yuanmou hominid fauna from Yunnan, southwestern China and its palaeoenvironmental implication. Journal of Palaeogeography 3, 323–330.

Denk, T., Grimm, G.W., Grímsson, F., Zetter, R., 2013. Evidence from "Köppen signatures" of fossil plant assemblages for effective heat transport of Gulf Stream to subarctic North Atlantic during Miocene cooling. Biogeosciences 10, 7927-7942.

Donders, T.H., Weijers, J.W.H., Munsterman, D.K., Kloosterboer-van Hoeve, M.L., Buckles, L.K., Pancost, R.D., Schouten, S., Sinninghe Damasté, J.S., Brinkhuis, H., 2009. Strong climate coupling of terrestrial and marine environments in the Miocene of northwest Europe. Earth and Planetary Science Letters 281, 215–225.

Erdei, B., Dolezych, M., Hably, L., 2009. The buried Miocene forest at Bükkábrány, Hungary. Review of Palaeobotany and Palynology 155, 69–79.

Figueiral, I., Mosbrugger, V., Rowe, N.P., Ashraf, A.R., Utescher, T., Jones, T.P., 1999. The Miocene peat-forming vegetation of northwestern Germany: an analysis of wood remains and comparison with previous palynological interpretations. Review of Paleobotany and Palynology 104, 239–266.

Frank, M.C., Bend, S.L., 2004. Preparation of Oriented Block Samples of Lignite for Petrographic Analysis. Journal of Sedimentary Research 74, 311–313.

Hatcher, P.G., Clifford, D.J. The organic geochemistry of coal: from plant materials to coal. Organic Geochemistry 5-6, 251-274.

Hudson, K., 2012. Uplift, denudation, and their causes and constraints over geological timescales. *In:* Roberts, D.G., Bally, R.A.W. (eds). Regional Geology and Tectonics: Principles of Geological Analysis. Elsevier, Amsterdam. 609–646.

Hámor-Vidó, M., Hofmann, T., Albert, L., 2010. In situ preservation and paleoenvironmental assessment of *Taxodiacea* fossil trees in the Bükkalja Lignite Formation, Bükkábrány open cast mine, Hungary. International Journal of Coal Geology 81, 203–210.

Hoffmann, P., Blanchette, R.A., 1997. The conservation of a fossil tree trunk. Studies in Conservation 42, 74–82.

Hudson, R.H., 1960. The anatomy of the genus Pinus in relation to its classification. Journal of the Institute of Wood Science 6, 26–46.

Hudspith, V.A. Belcher, C.M., 2020. Some semifusinite in coal may form during diagenesis, not wildfires. International Journal of Coal Geology 218, 103360.

Ickert-Bond, S.M., 2001. Reexamination of wood anatomical features in *Pinus krempfii* (Pinaceae). IAWA Journal 22, 355–265.

International Committee for Coal and Organic Petrology (ICCP), 2001. The new inertinite classification (ICCP System 1994). Fuel 80, 459–471.

Ireland, A.W., Booth, R.K., 2011. Hydroclimatic variability drives episodic expansion of a floating peat mat in a North American glacial kettle. Ecology 92, 11–18.

Ireland, A.W., Booth, R.K., Hotchkiss, S.C., Schmitz, J.E., 2012. Drought as a trigger for rapid state shifts in kettle ecosystems: implications for ecosystem responses to climate change. Wetlands 32, 989–1000.

Ireland, A.W., Booth, R.K., Hotchkiss, S.C., Schmitz, J.E., 2013. A comparative study of within-basin and regional peatland development: implications for peatland carbon dynamics. Quaternary Science Reviews 71, 85–95.

Jeong, E.K., Kim, K., Suzuki, M., Uemura, K., 2012. Daijima-type conifer wood assemblage of the Hatamura Formation (Middle Miocene) in the Akita Prefecture, Japan. Geosciences Journal 16, 115–125.

Jewell, R.B., 2004. The sedimentation, stratigraphy, and petrography of a coal-ash pond in Carroll County, Kentucky. Unpublished M.S. thesis. University of Kentucky, Lexington, KY, 156 p.

Korasidis, V.A., Wallace, M.W., Wagstaff, B.E., Holdgate, G.R., Tosolini, A.-M.P., Jansen, B., 2016. Cyclic floral succession and fire in a Cenozoic wetland/peatland system. Palaeogeography Palaeoclimatology Palaeoecology 461, 237–252.

Logan, K.J., Thomas, B.A., 1987. The distribution of lignin derivatives in fossil plants. New Phytologist 105, 157–173.

López-Buendía, A.M., 1998. A new method for the preparation of peat samples for petrographic study by transmitted and reflected light microscopy. Journal of Sedimentary Research 68, 214–217.

MacParland, L.C., Collinson, M.E., Scott, A.C., Campbell, G., 2009. The use of reflectance values for the interpretation of natural and anthropogenic charcoal assemblages. Archaeology and Anthropological Science 1, 249–261.

Mantzouka, D., Sakala, J., Kvaček, Z., Koskeridou, E., Ioakim, C., 2019. Two fossil conifer species from the Neogene of Alonissos Island (Iliodroma, Greece). Geodiversitas 41, 125–142.

Mukhopadhyay, P.K., 1994. Vitrinite reflectance as maturity parameter: petrographic and molecular characterization and its applications to basin modeling. In: Mukhopadhyay, P.K., Dow, W. (eds.). Vitrinite Reflectance as a Maturity Parameter. ACS Symposium Series; American Chemical Society, Washington, D.C., 1–24.

Mustoe, G.E., 2018. Non-mineralized fosssil wood. Geosciences 8, 233. https://doi10.3390/geosciences8060223.

Pickel, W, Kus, J., Flores, D., Kalaitzidis, S., Christanis, K., Cardott, B.J., Misz-Kennan, M., Rodrigues, S., Hentschel, A., Hamor-Vido, M., Crosdale, P., Wagner, N., ICCP, 2017. Classification of lipinite - ICCP system 1994. International Journal of Coal Geology 169, 40–61.

Pound, M.J., Riding, J.B., 2016. Palaeoenvironment, palaeoclimate and age of the Brassington Formation (Miocene) of Derbyshire, UK. Journal of the Geological Society 173, 306–319.

Pound, M.J., Riding, J.B., Donders, T.H., Daskova, J., 2012a. The palynostratigraphy of the Brassington Formation (Upper Miocene) of the southern Pennines, central England. Palynology 36, 26–37.

Pound, M.J., Haywood, A.M., Salzmann, U., Riding, J.B., 2012b. Global vegetation dynamics and latitudinal temperature gradients during the Mid to Late Miocene (15.97–5.33Ma). Earth-Science Reviews 112, 1-22.

Pound, M.J., O'Keefe, J.M.K., Nuñez Otaño, N.B., Riding, J.B., 2019. Three new Miocene fungal palynomorphs from the Brassington Formation, Derbyshire, UK. Palynology 43, 596–607.

Quan, C., Liu, Y.-S., Tang, H., Utescher, T., 2014. Miocene shift of European atmospheric circulation from trade wind to westerlies. Scientific Reports 4, 5660

Richter, H.G., Grosser, D., Heinz, I., Gasson, P.E. (eds.). 2004. IAWA list of microscopic features for softwood identification. IAWA Journal 25, 1–70.

Scott, A.C., 2018. Burning Planet: the story of fire through time. Oxford University Press, 256p.

Scott, A.C., 2009. The Pre-Quaternary history of fire. Palaeogeography, Paleoclimatology, Palaeoecology 164, 281–329.

Smith, A., 2013. Digital Geological Map of Great Britain, information notes, 2013. British Geological Survey Open Report, OR/13/007. 54pp.

Sýkorová, I., Pickel, W., Christanis, K., Wolf, M., Taylor, G.H. Flores, D., 2005. Classification of huminite - ICCP System 1994. International Journal of Coal Geology 62, 85–106.

Van der Burgh, J., 1973. Hölzer der Niederrhenischen Braunkohlenformation. 2. Review of Palaeobotany and Palynology 15, 73–275

Vane, C.H. 2003a. Monitoring decay of black gum (*Nyssa sylvatica*) wood during growth the shiitake mushroom (*Lentinula edodes*) using DRIFT spectroscopy. Applied Spectroscopy 57, 5, 514-517.

Vane, C.H. 2003b. The molecular composition of lignin in spruce decayed by white-rot fungi (*Phanerochaete chrysosporium* and *Trametes versicolor*) using Pyrolysis–GC-MS and Thermochemolysis with Tetramethylammonium Hydroxide. International Biodeterioration and Biodegradation 51, 1, 67-75.

Vane, C.H., Abbott, G.D., 1999. Proxies for land plant biomass: Closed system microscale pyrolysis of some methoxyphenols. Organic Geochemistry 30, 1535-1541.

Vane, C.H., Drage, T.C., Snape, C.E. 2006. Bark Decay by the white-rot fungus *Lentinula edodes*: Polysaccharide loss, lignin resistance and the unmasking of suberin. International Biodeterioration and Biodegradation 57, 14-23.

Vane, C.H., Abbott, G.D., Head, I.M., 2001a. The effect of fungal decay (*Agaricus bisporus*) on wheat straw lignin using pyrolysis-GC-MS in the presence of tetramethylammonium hydroxide (TMAH). Journal of Analytical and Applied Pyrolysis 60, 1, 69-78.

Vane, C.H., Martin, S.C, Snape, C.E., Abbott, G.D. 2001b. Degradation of lignin in wheat straw during growth of the Oyster mushroom (*Pleurotus ostreatus*) using off-line thermochemolysis with tetramethylammonium hydroxide and solid state ^{13}C NMR. Journal of Agriculture and Food Chemistry 49, 2709-2716.

Walsh, P.T., Banks, V.J., Jones, P.F., Pound, M.J., Riding, J.B., 2018. A reassessment of the Brassington Formation (Miocene) of Derbyshire, UK and a review of related hypogene karst suffosion processes. Journal of the Geological Society 175, 443–462.

Walsh, P.T., Boulter, M.C., Ijtaba, M., Urbani, D.M. 1972. The preservation of the Neogene Brassington Formation of the southern Pennines and its bearing on the evolution of upland Britain. Journal of the Geological Society 128, 519–559.

Walsh, P.T., Collins, P., Ijtaba, M., Newton, J.P., Scott, N.H., Turner, P.R., 1980. Palaeocurrent directions and their bearing on the origin of the Brassington Formation (Miocene-Pliocene) of the Southern Pennines, Derbyshire, England. The Mercian Geologist 8, 47-62.

Wang, H.-B., Oskolski, A.A., Jacques, F.M.B., Wang, Y.-H., Zhou, Z.-K., 2017. Lignified woods of *Pinus* (Pinaceae) from the late Miocene of central Yunnan, China, and their biogeographic and paleoclimatic implications. Palaeoworld 26, 553–565.

Yorke, C. 1954. *The pocket deposits of Derbyshire*. Privately published, Birkenhead, three volumes.

Yorke, C. 1961. *The pocket deposits of Derbyshire. A general survey*. Privately published, Birkenhead.

Table Captions:

Table 1. Macroscopic descriptions of the samples examined in this study. All wood and lignite samples are from Kenslow Member sediments exposed in Bees Nest Pit, Derbyshire, UK.

Table 2. Random textinite (uncharred), vitrinite (transition), and fusinite/semifusinite (charred) reflectance for selected samples of drift woods and lignite.

Table 3. Maceral and mineral matter compositions through the lignite bed profile, reported as 0.9 cm aggregates of counts spaced 0.3 mm vertically along each of 10 transects through the column (pillar) sample of lignite.

Table 4. Results of bulk elemental organic geochemistry showing the atomic H:C and O:C ratios.

Figure Captions:

Figure 1. Map illustrating the locations of Bees Nest Pit and Kenslow Top Pit in the southern Pennines, Derbyshire, UK. The materials studied herein are all from Bees Nest Pit. The Kenslow Member at Kenslow Top Pit is no longer exposed. Yellow outcrop pattern of the Brassington Formation is based upon British Geological Survey 1:10000 scale digital geological map (Smith, 2013; Using: EDINA Geology Digimap Service, <https://digimap.edina.ac.uk>, Downloaded: 2020-02-27). Notable settlements are identified in grey text. Inset map of the British Isles showing the location (star) of the aerial image (High Resolution (25cm) Vertical Aerial Imagery, Scale 1:500, Getmapping, Using: EDINA Aerial Digimap Service, <https://digimap.edina.ac.uk>).

Figure 2. Stratigraphy of Bees Nest Pit. a) field photograph of the north wall of Bees Nest Pit showing all three members. b) simplified stratigraphy of the Brassington Formation based on Walsh et al. (1980). c) simplified stratigraphy of the 2019 measured section showing the distribution of wood through the lignite and grey clay. Size of the wood image reflects the size of wood fossils recovered.

Figure 3. SEM images of NU13-001 and charred fragments thereof. a–c) wood that appears undamaged in hand sample contains collapsed, homogenized cells when viewed at successively higher magnification (655x, 1,820x, 17,900x, respectively). d–f) NU13-002 lightly charred wood in transverse section showing growth rings and radial pitting at successively higher magnifications (437x, 1,820x, 18,000x respectively). Note the height of the rings and the lack of differentiation between earlywood and latewood. g–i) NU13-003 lightly charred wood in radial

to tangential section showing rays and uniseriate pits at successively higher magnifications (714x, 1,450x, and 1,460x, respectively).

Figure 4. Images illustrating variations in preservation in disseminated wood sample JOMSUGL 908 a) view of transverse section showing fibers surrounding a detrovitrinite and semifusinite filled pocket. b) tangential section showing a pattern of two rays between each tracheid; note that tracheids appear brighter than the rays. c) radial section in the interior of the wood fragment showing largely unaltered wood retains significant red and gold internal refections; note two visible uniseriate scleriform pits. d) transverse view somewhat interior to (a) showing separated fibers with huminitic-semifusinitic material filling the spaces between the cells. e) the same view in blue light epifluorescence showing cracks in the fiber cells and dim yellow fluorescence. F) transverse view further toward the middle of the wood sample showing swollen, cracked, and delaminated fiber cells. Scale bar = 100 micrometers.3 a–d) photomicrographs were made in reflected white illumination with an oil immersion objective. 3 e–f) images were made with blue light excitation with an oil immersion objective.

Figure 5. White light-blue light illumination pairs in oil immersion showing the effects of white rot fungal invasion of the disseminated wood from sample JOMSUGL 908. a) blue light image showing loss of fluorescence of collapsed cells as cellulose and lignin are sequentially lost. b) same view in white light showing early huminite maceral development with remnant internal reflections. c) blue light image of less collapsed cells showing degraded and pitted layers surrounded by weaker-fluorescing collapsed material. d) same field of view as (c) in white light showing darkening of the remnant cell walls and loss of internal reflections, but not yet incipient maceral development.

Figure 6. Examples of other macerals occuring in the clay surrounding the dispersed wood samples. 6a, f-g are from sample JOMSUGL 908. 6b, d-e are from sample JOMSUGL 909. 6c is from sample JOMSUGL 910. a) funginite produced by a fungal sclerotia; b) funginite likely produced by a helicosporous conidium; c) cutinite (under epifluorescence); d) sporinite as the corpus of a bisaccate pollen grain; e) sporinite (under epifluorescence) as a monolete or monosulcate grain; f) textinite; g) Ulminite A&B. Scale bars = 100 micrometers. 4 a-b-d-f-g photomicrographs were made in reflected white illumination in oil immersion. 4 c-e) images were made with blue light excitation in oil immersion.

Figure 7. Mineral matter and maceral composition of the lignite lentil contained in the sedimentary profile. Spacing is 0.9 cm through the column (pillar) sample.

Figure 8. Variations in huminite maceral composition through the lignite lentil. Spacing is 0.9 cm through the column (pillar) sample.

Figure 9. Example macerals and minerals present in the lignite lentil a) textinite B and ulminite B grading into each other across a vertical transect through one piece of wood in the lignite, 8.1 cm depth. b) texinite A in a clay matrix, 4.5 cm depth. c) phlobaphinites as a rootlet in clay, 5.4 cm depth. d) phlobaphinite in suberinite, 5.4 cm depth. e) funginite (small white circles) in ulminite (the exposure and color balance were adjusted to highlight the funginite; the image as printed is not representative of the relative reflectance of the lignite), 3.6 cm depth. f) fusinite, 9.9 cm depth. g) suberinite surrounding dark-appearing phlobaphinites, 5.4 cm depth (photo pair with d). h) cutinite with resinite, 24.3 cm depth. Scale bars = 100 micrometers. Photomicrographs 7 a−f were taken with reflected white illumination in oil immersion. Photomicrographs 7 g−h) images were made with blue light epifluorescence in oil immersion.

Figure 10. Key features in identifying the xylitic disseminated wood in sample JOMSUGL 908. Left images are in white reflected light illumination in oil immersion; right images are in blue light excitation showing epifluorescence in oil immersion. a–d) transverse sections showing uniseriate to parallel biseriate tracheids. e–f) radial section showing ray cells; ray cells are always in groups of three. g–h) transverse section showing uncommon cupressiod-taxodioid pits Scale bars = 100 micrometers.

Figure 11. van Krevelen bi-plot of elemental ratios of Kenslow Member fossil woods (diamonds) and exemplar modern woods and coals. Generalized areas for modern, fossil, low rank coalification (Lignite-Brown coal) and early-mid coalificatiion (Sub-bituminous) are shown to highlight that the Kenslow Member fossil woods are at a very early stage of alteration within the overall wood-coal continuum.

Table 1.

Sample Number	Collection Date	Collection Held In	Relative Location in the Kenslow Member	Macroscopic Description
NU13-001	2013	Northumbria University	Upper Kenslow	Disseminated bolt of wood, approximately 60 cm cm x20 cm lacking bark. Bolt exterior is dark grey interior is reddish-brown. Originally coated in gr Exterior and internal cracking present; clay coati extends into cracks.
NU13-002	2013	Northumbria University	Upper Kenslow	Charred fragment from NU13-001, 0.5cm x 0.5cm 0.2cm. Black in colour throughout. Originally coat grey clay.
NU13-003	2013	Northumbria University	Upper Kenslow	Charred fragment from NU13-001, 1cm x 0.7cm x Black in colour throughout. Originally coated in g clay.
JOMSUGL 908	Jun-17	Morehead State University	Middle Kenslow	Disseminated small branch, 27 cm x 15 cm x15 cr in color throughout. Originally coated in grey clay Exterior cracking present; clay coating extends in cracks.
JOMSUGL 909	Jun-17	Morehead State University	Middle Kenslow	Disseminated small branch, 24 cm x 6 cm x 3 cm. in color throughout. Originally coated in grey clay visible cracking.
JOMSUGL 910	Jun-17	Morehead State University	Middle Kenslow	Disseminated small length of wood, 18 cm x 7.5 c cm. Black in color throughout. Originally coated i clay. Cracking resulting in sub-centimeter "layeri parallel to the long axis; clay coating extends into
JOMSUGL 1245 & 1246	Jul-19	Morehead State University	Upper Kenslow	Oriented column (pillar) sample through the ligni lentil above the woodground in the Kenslow Mem Column is from the nothern margin of the lentil. T column is 26.8 cm thick and consists from bottom 4.8 cm of burrowed white and grey clay with abu wood fragments; 1 cm bone coal; 1.1 cm cm fusai (charcoal); 3.8 cm bone coal; 1 cm sub-vitrain (da brown dull wood); 0.3 cm bone coal; 1 cm fusain; bone coal; 3.1 cm vitrain (black glossy wood); 2.3 bone coal; 0.8 cm vitrain (black glossy wood); 1.1 sub-vitrain (glossy dark red-brown wood); 2.2 cm coal with white clay-filled burrows; 3.2 cm white clay. Block sample JOMSUGL 1245 is the upper 1 and JOMSUGL 1246 is the lower 13.8 cm of the co
OG 100	Oct-13	British Geological Survey	Middle Kenslow	Disseminated small length of wood, 10 cm x 7.5 c cm. Tan brown in color throughout. Originally coa grey clay; clay coating extends into cracks.
OG11	Oct-13	British Geological Survey	Middle Kenslow	Disseminated small branch, 14 cm x 4 cm x 3 cm. Brown in color throughout. Originally coated in g clay. Exterior cracking present; clay coating exten cracks.

OG7	Oct-13	British Geological Survey	Middle Kenslow	Disseminated small branch, 20 cm x 9 cm x 4 cm. brown in color throughout. Originally coated in g clay. Exterior cracking present;
OG10a	Oct-13	British Geological Survey	Middle Kenslow	Disseminated small length of wood, 5 cm x 4 cm x Tan brown in color throughout. Some root in-gro (removed) Originally coated in grey clay. Exterio cracking present; clay coating extends into crack
OG10b	Oct-13	British Geological Survey	Middle Kenslow	Wood fragment, 5 cm x 4 cm x 2 cm. Tan brown i throughout. Originally coated in grey clay. Exteri cracking present; clay coating extends into crack
OG21	Oct-13	British Geological Survey	Middle Kenslow	Disseminated small branch, 14 cm x 10 cm x 6 cm brown in color throughout. Originally coated in g clay. Exterior cracking present; clay coating exte cracks.
OG13	Oct-13	British Geological Survey	Middle Kenslow	Disseminated wood, 11 cm x 7 cm x 5 cm. Tan bro color throughout. Cubic cracking on surface only. Originally coated in grey clay. Exterior cracking p clay coating extends into cracks.
OG101	Oct-13	British Geological Survey	Middle Kenslow	Disseminated small branch, 14 cm x 9 cm x 5 cm. brown in color throughout. Originally coated in g clay. Exterior cracking present; clay coating exte cracks.

Table 2.

	Random Reflectance (%Ro (st.dev.) n=measurements made)		
Sample	Charred (inertinite)	Transition (high reflecting huminite)	Uncharred (low reflecting huminite)
908, transverse section	0.98 (0.13); n=34	0.53 (0.08); n=43	0.20 (0.08); n=112
908, radial section	-	-	0.14 (0.03); n=100
909, transverse section	-	-	0.10 (0.06); n=41
910, transverse section	-	-	0.31 (0.04); n=100
1245-2	2.87 (0.27); n=20	-	0.21 (0.07); n=30
1246-1	-	-	0.19 (0.05); n=100

Table 3.

	Mineral Matter			Huminite						Inertinite			Liptini		
				Telo-huminite		Gelo-huminite		Detro-huminite							
Depth in cm	Clay	Quartz silt & sand	Pyrite	Textinite	Ulminite	Corpogelinite	Gelinite	Attrinite	Densinite	Fusinite	Semifusinite	Funginite	Sporinite	Cutinite	
0.9	97.0%	0.0%	0.0%	0.0%	0.0%	0.0%	0.0%	0.0%	1.0%	0.0%	0.0%	0.0%	0.0%	2.0%	
1.8	96.2%	2.2%	0.0%	0.0%	0.5%	0.0%	0.0%	0.0%	0.5%	0.0%	0.0%	0.0%	0.5%	0.0%	
2.7	93.6%	3.2%	0.0%	0.0%	0.0%	0.0%	0.0%	0.0%	0.5%	0.0%	0.0%	1.1%	1.6%	0.0%	
3.6	90.3%	4.3%	0.0%	0.0%	1.9%	0.0%	0.0%	0.0%	0.4%	0.0%	0.0%	1.2%	1.9%	0.0%	
4.5	80.3%	2.3%	0.0%	1.7%	0.3%	0.0%	0.0%	0.0%	14.0%	0.0%	0.0%	1.0%	0.3%	0.0%	
5.4	76.5%	2.0%	0.0%	1.3%	4.0%	0.7%	0.0%	0.0%	13.2%	0.7%	0.3%	0.0%	0.7%	0.0%	
6.3	74.0%	2.1%	0.0%	0.7%	10.4%	0.7%	0.0%	0.0%	5.2%	2.1%	0.0%	0.3%	0.3%	0.7%	
7.2	45.7%	0.4%	0.4%	2.2%	43.9%	0.0%	0.0%	0.0%	2.7%	0.4%	0.0%	0.4%	0.9%	0.0%	
8.1	14.7%	0.0%	0.7%	0.7%	76.6%	0.0%	0.0%	0.0%	0.0%	0.0%	0.0%	0.0%	1.3%	0.0%	
9	33.5%	1.9%	0.0%	1.3%	45.0%	0.0%	0.0%	5.3%	5.3%	0.3%	0.0%	0.0%	1.7%	1.1%	
9.9	61.1%	6.7%	0.0%	0.3%	7.6%	0.0%	0.0%	7.3%	7.3%	3.3%	0.0%	0.0%	2.5%	2.2%	
10.8	71.2%	1.3%	0.3%	2.0%	2.1%	0.8%	0.0%	6.5%	6.5%	0.0%	0.7%	0.0%	1.7%	3.4%	
11.7	31.6%	0.0%	0.0%	1.1%	55.0%	0.4%	0.0%	2.6%	2.9%	0.0%	0.0%	0.0%	1.1%	0.5%	
12.6	2.4%	0.7%	0.0%	0.0%	86.8%	1.3%	0.0%	0.0%	0.0%	0.0%	0.0%	0.0%	0.0%	0.0%	
13.5	5.6%	2.0%	0.0%	0.0%	87.1%	2.3%	0.0%	0.0%	0.0%	0.0%	0.4%	0.0%	0.0%	0.0%	
14.4	8.5%	0.5%	0.0%	0.0%	83.8%	0.8%	0.0%	0.0%	0.0%	0.0%	0.5%	0.0%	0.0%	0.0%	
15.3	7.0%	0.0%	0.0%	0.0%	86.7%	3.3%	2.3%	0.0%	0.0%	0.0%	0.0%	0.0%	0.0%	0.0%	
16.2	7.0%	0.0%	0.0%	0.0%	86.7%	3.3%	2.3%	0.0%	0.0%	0.0%	0.0%	0.0%	0.0%	0.0%	
17.1	3.9%	0.0%	0.0%	3.9%	82.4%	7.8%	0.0%	0.0%	0.0%	0.0%	0.0%	0.0%	0.0%	0.0%	
18	56.5%	1.3%	0.0%	13.4%	5.6%	2.6%	3.3%	0.0%	8.6%	0.0%	4.6%	0.0%	1.6%	1.3%	
18.9	15.7%	1.6%	0.0%	54.6%	1.7%	0.0%	5.2%	0.0%	0.7%	0.0%	7.2%	0.0%	0.0%	0.0%	1
19.8	12.3%	2.5%	0.0%	61.5%	0.6%	0.0%	1.7%	0.0%	2.3%	0.0%	2.2%	0.0%	0.0%	0.0%	1
20.7	37.7%	0.0%	0.0%	36.2%	0.4%	0.0%	8.2%	0.0%	1.3%	0.0%	13.9%	0.0%	0.0%	0.4%	
21.6	57.9%	0.9%	0.0%	24.7%	0.5%	2.2%	3.3%	0.0%	1.9%	0.0%	3.7%	0.0%	0.9%	1.3%	
22.5	62.7%	2.4%	0.0%	14.0%	0.8%	2.6%	0.0%	0.0%	5.9%	0.0%	0.5%	0.0%	0.5%	4.7%	
23.4	51.3%	0.4%	0.0%	20.3%	1.1%	7.0%	2.9%	0.0%	3.9%	0.0%	0.0%	0.0%	0.4%	3.5%	
24.3	63.2%	0.0%	0.0%	18.5%	0.8%	2.5%	0.0%	0.0%	0.4%	0.0%	0.0%	0.0%	0.4%	11.5%	
25.2	44.9%	2.0%	0.0%	13.1%	3.9%	12.5%	0.0%	0.0%	0.9%	0.0%	0.0%	0.0%	0.6%	8.1%	
26.1	44.7%	0.6%	0.0%	18.5%	0.6%	13.2%	2.7%	0.0%	0.0%	0.0%	0.0%	0.0%	1.2%	6.4%	
27	41.4%	0.4%	0.0%	25.6%	0.4%	10.3%	0.9%	0.0%	0.3%	0.0%	1.6%	0.0%	0.4%	6.1%	
27.9	18.9%	0.0%	0.0%	63.1%	0.7%	3.4%	1.9%	0.0%	0.0%	0.0%	5.5%	0.0%	0.0%	0.0%	
28.8	41.6%	0.7%	0.0%	37.6%	1.6%	1.7%	0.0%	0.0%	0.0%	0.0%	0.4%	0.0%	0.4%	0.0%	
29.7	63.9%	0.4%	0.0%	3.6%	0.9%	4.4%	0.0%	0.0%	0.5%	0.0%	0.5%	0.0%	1.0%	1.9%	

30.6	77.6%	0.5%	0.0%	4.6%	0.0%	2.8%	0.0%	0.0%	0.0%	0.0%	0.0%	1.1%	0.0%	0.0%

Table 4.

Sample I.D.	Carbon %	Hydrogen %	Nitrogen %	Oxygen %	Ash %	Atomic H:C	Atomic O:C
OG7	57.87	5.62	1.02	35.49	2.56	1.17	0.46
OG10a	58.66	5.78	1.11	30.64	3.77	1.18	0.39
OG10b	60.49	6.06	1.13	32.31	1.82	1.20	0.40
OG11	59.11	5.55	0.00	35.34	4.28	1.13	0.44
OG13	57.15	5.94	0.00	36.91	0.74	1.25	0.48
OG21	53.68	5.83	0.00	40.48	3.79	1.31	0.57
OG100	52.82	3.38	0.11	43.68	24.40	0.77	0.62
OG101	38.32	3.42	0.01	58.20	37.59	1.15	0.46

CRediT author statement

J. O'Keefe was part of the field investigative team, completed all organic petrographic and paleobotanical analyses and interpretation, led the writing of the original manuscript, and was in charge of the revision.

M. Pound was part of the field investigative team, completed all SEM analyses, contributed significantly to the writing of the original manuscript, and contributed to the revision.

J. Riding was part of the field investigative team, contributed significantly to the writing of the original manuscript, and contributed to the revision.

C. Vane contributed organic geochemical analyses and discussion to the revised manuscript and contributed to the revision.

Declaration of interests

☒ The authors declare that they have no known competing financial interests or personal relationships that could have appeared to influence the work reported in this paper.

Highlights

- First study of Miocene-age wood and lignite from the Kenslow Member of the Brassington Formation, Derbyshire, UK.
- Lignite rank is Lignite B; wood rank is Peat.
- Wood is preserved as mummifications that show a range of fire and fungal impacts.
- Wood appears to be from Pinnaceae or Cupressaceae.

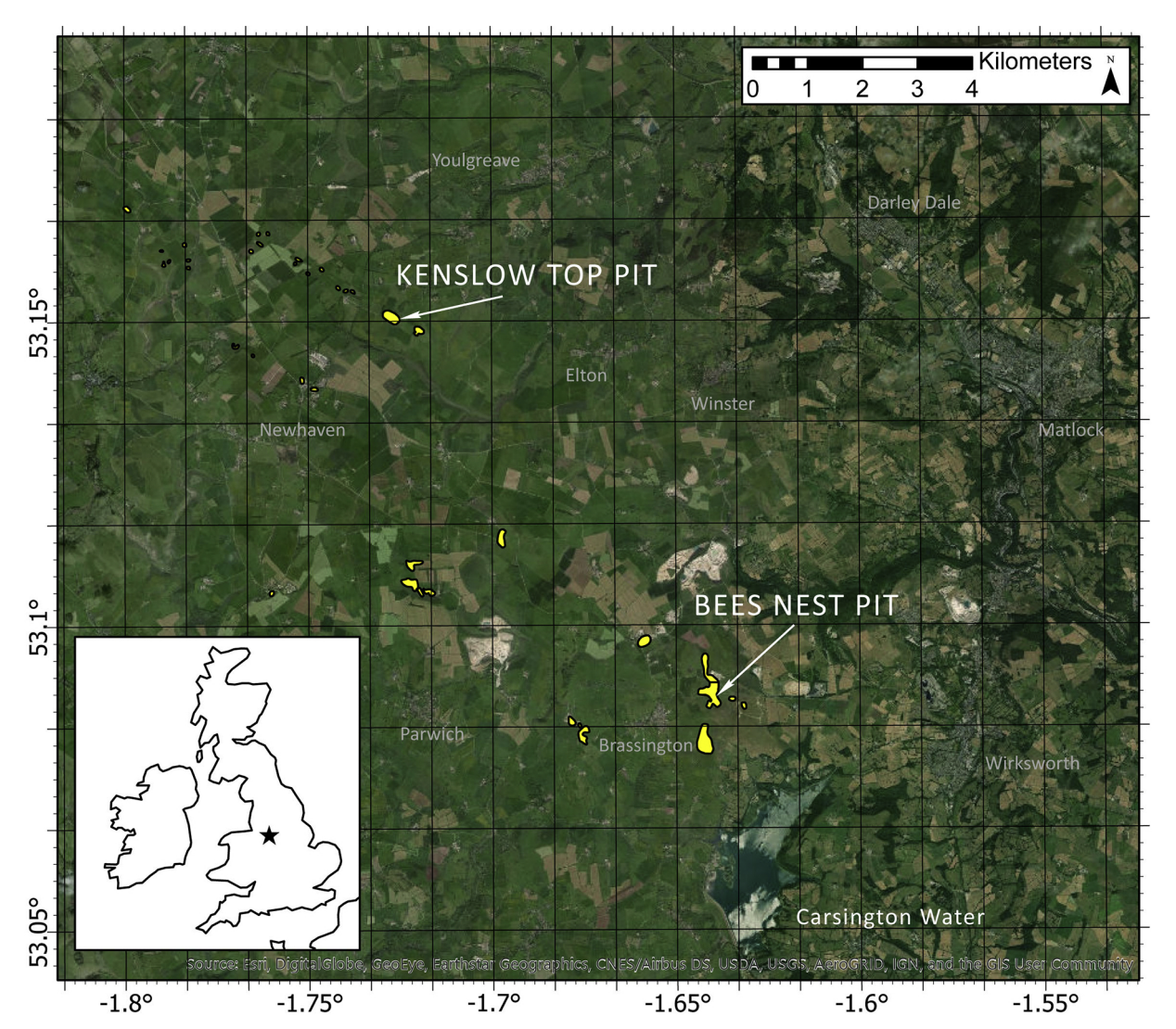
Kilometers
0 1 2 3 4
N
Youlgreave
Darley Dale
KENSLOW TOP PIT
Elton
Winster
Newhaven
Matlock
BEES NEST PIT
Parwich
Brassington
Wirksworth
Carsington Water
53.15°
53.1°
53.05°
-1.8°
-1.75°
-1.7°
-1.65°
-1.6°
-1.55°
Source: Esri, DigitalGlobe, GeoEye, Earthstar Geographics, CNES/Airbus DS, USDA, USGS, AeroGRID, IGN, and the GIS User Community

Figure 1

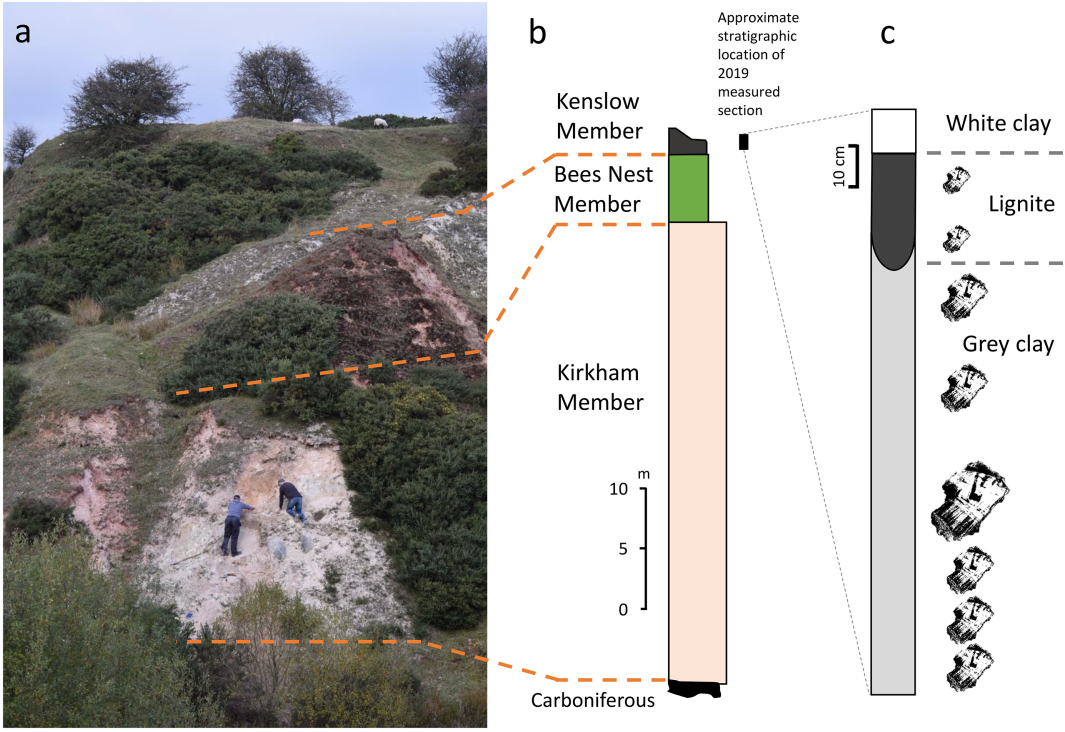
a
b
Approximate stratigraphic location of 2019 measured section
c
Kenslow Member
Bees Nest Member
Kirkham Member
m
10
5
0
Carboniferous
10 cm
White clay
Lignite
Grey clay

Figure 2

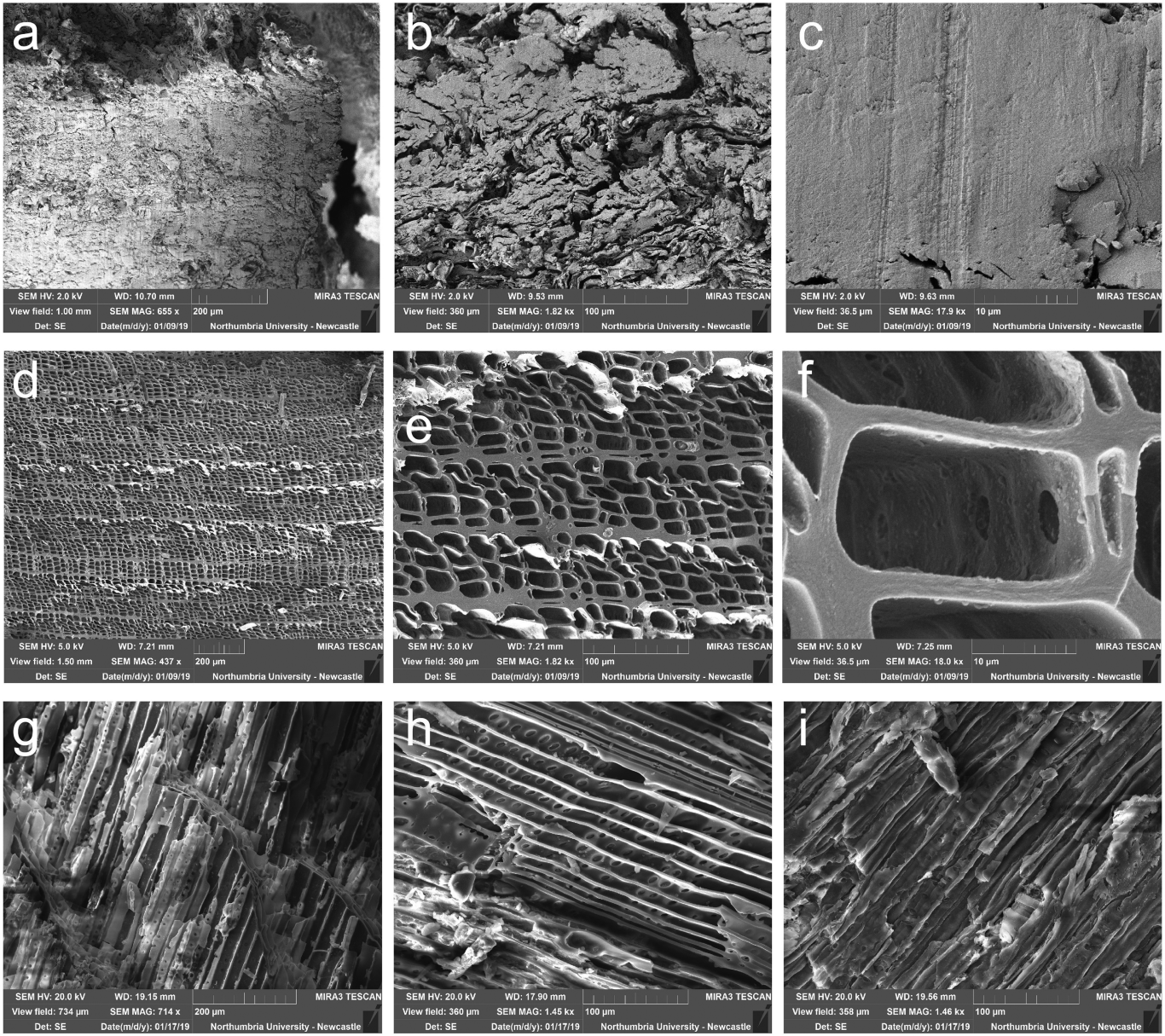
a
SEM HV: 2.0 kV WD: 10.70 mm MIRA3 TESCAN
View field: 1.00 mm SEM MAG: 655 x 200 µm
Det: SE Date(m/d/y): 01/09/19 Northumbria University - Newcastle
b
SEM HV: 2.0 kV WD: 9.53 mm MIRA3 TESCAN
View field: 360 µm SEM MAG: 1.82 kx 100 µm
Det: SE Date(m/d/y): 01/09/19 Northumbria University - Newcastle
c
SEM HV: 2.0 kV WD: 9.63 mm MIRA3 TESCAN
View field: 36.5 µm SEM MAG: 17.9 kx 10 µm
Det: SE Date(m/d/y): 01/09/19 Northumbria University - Newcastle
d
SEM HV: 5.0 kV WD: 7.21 mm MIRA3 TESCAN
View field: 1.50 mm SEM MAG: 437 x 200 µm
Det: SE Date(m/d/y): 01/09/19 Northumbria University - Newcastle
e
SEM HV: 5.0 kV WD: 7.21 mm MIRA3 TESCAN
View field: 360 µm SEM MAG: 1.82 kx 100 µm
Det: SE Date(m/d/y): 01/09/19 Northumbria University - Newcastle
f
SEM HV: 5.0 kV WD: 7.25 mm MIRA3 TESCAN
View field: 36.5 µm SEM MAG: 18.0 kx 10 µm
Det: SE Date(m/d/y): 01/09/19 Northumbria University - Newcastle
g
SEM HV: 20.0 kV WD: 19.15 mm MIRA3 TESCAN
View field: 734 µm SEM MAG: 714 x 200 µm
Det: SE Date(m/d/y): 01/17/19 Northumbria University - Newcastle
h
SEM HV: 20.0 kV WD: 17.90 mm MIRA3 TESCAN
View field: 360 µm SEM MAG: 1.45 kx 100 µm
Det: SE Date(m/d/y): 01/17/19 Northumbria University - Newcastle
i
SEM HV: 20.0 kV WD: 19.56 mm MIRA3 TESCAN
View field: 358 µm SEM MAG: 1.46 kx 100 µm
Det: SE Date(m/d/y): 01/17/19 Northumbria University - Newcastle

Figure 3

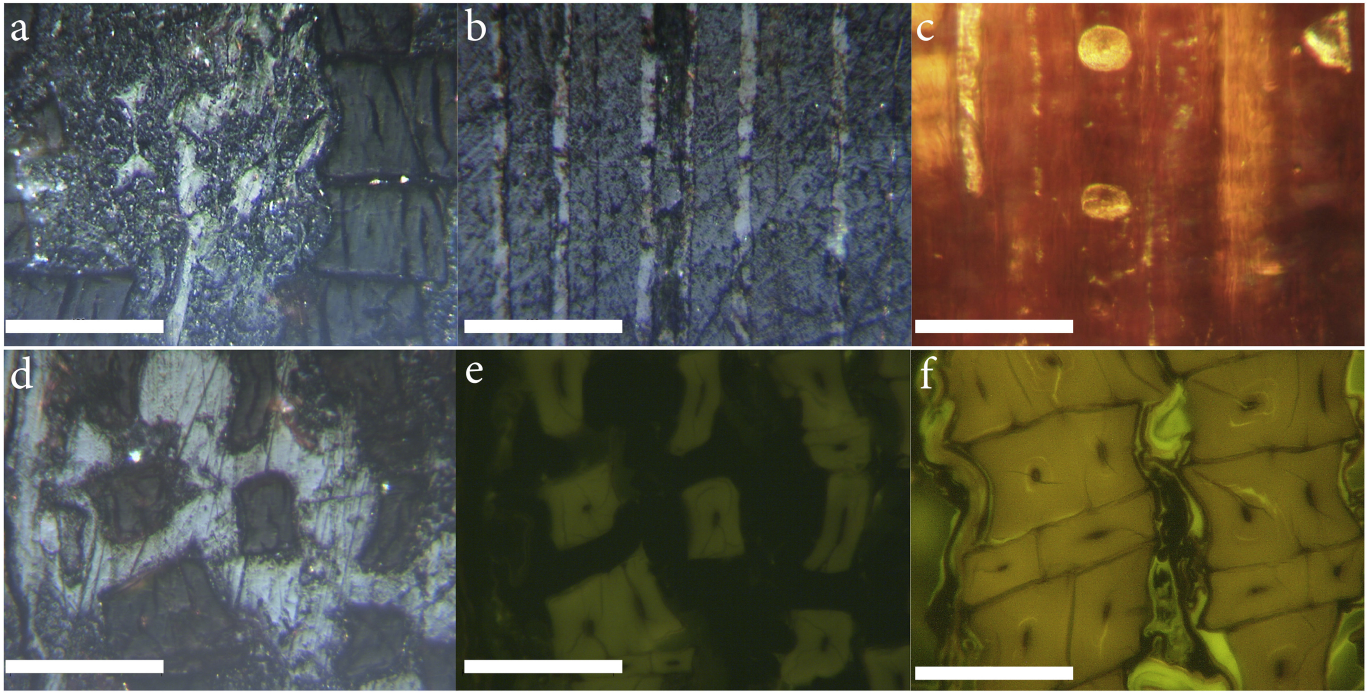

Figure 4

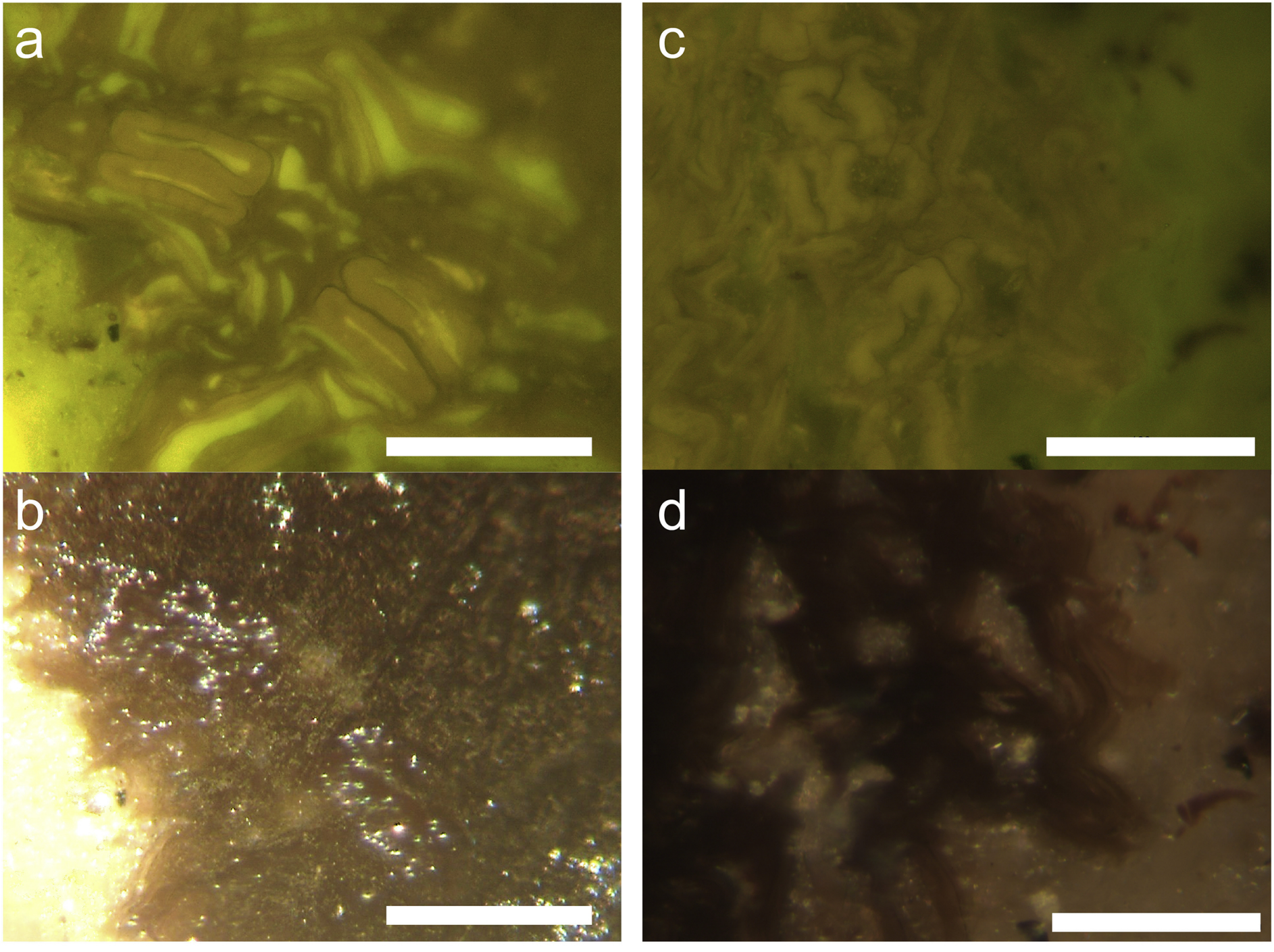

Figure 5

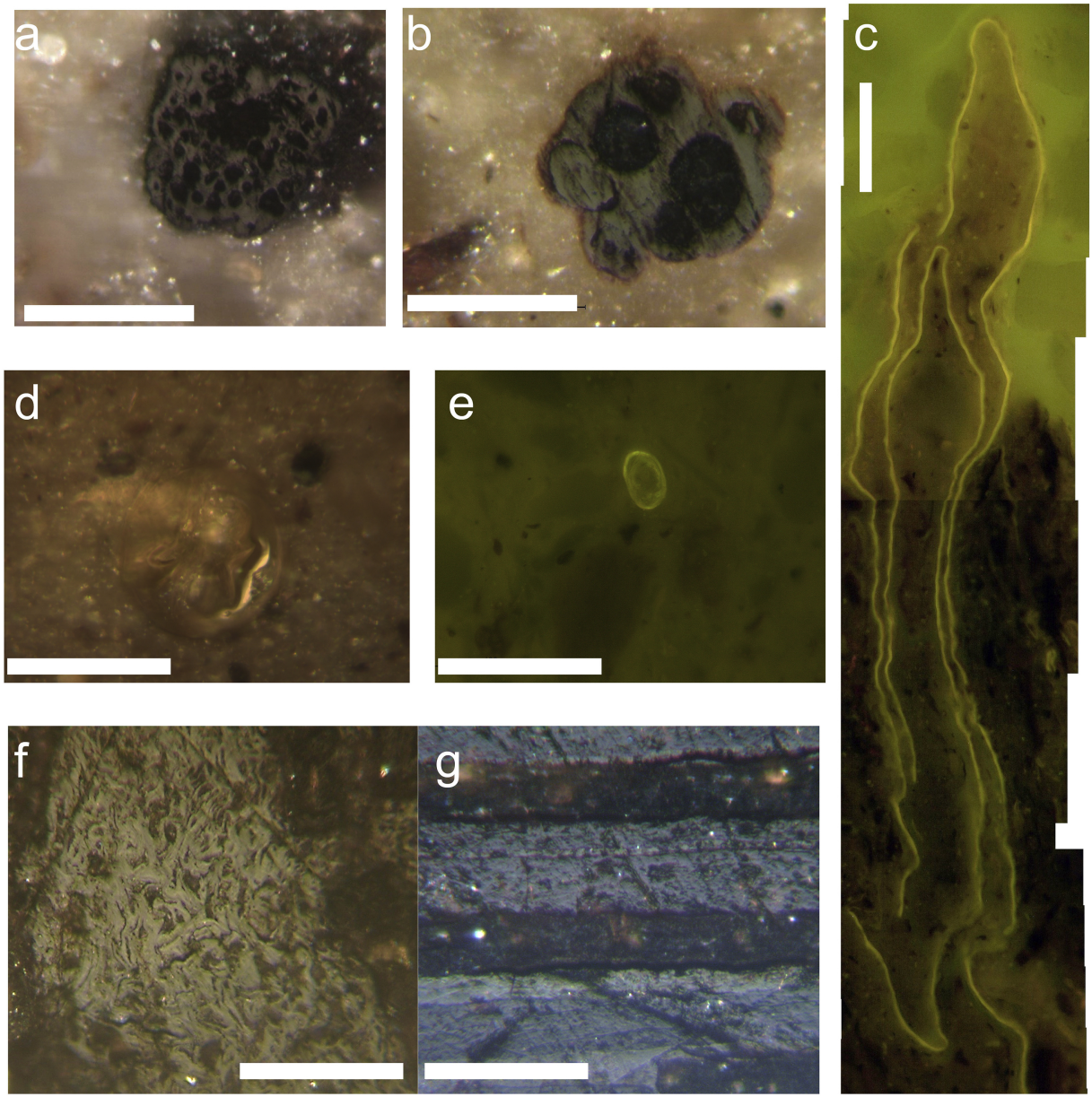

Figure 6

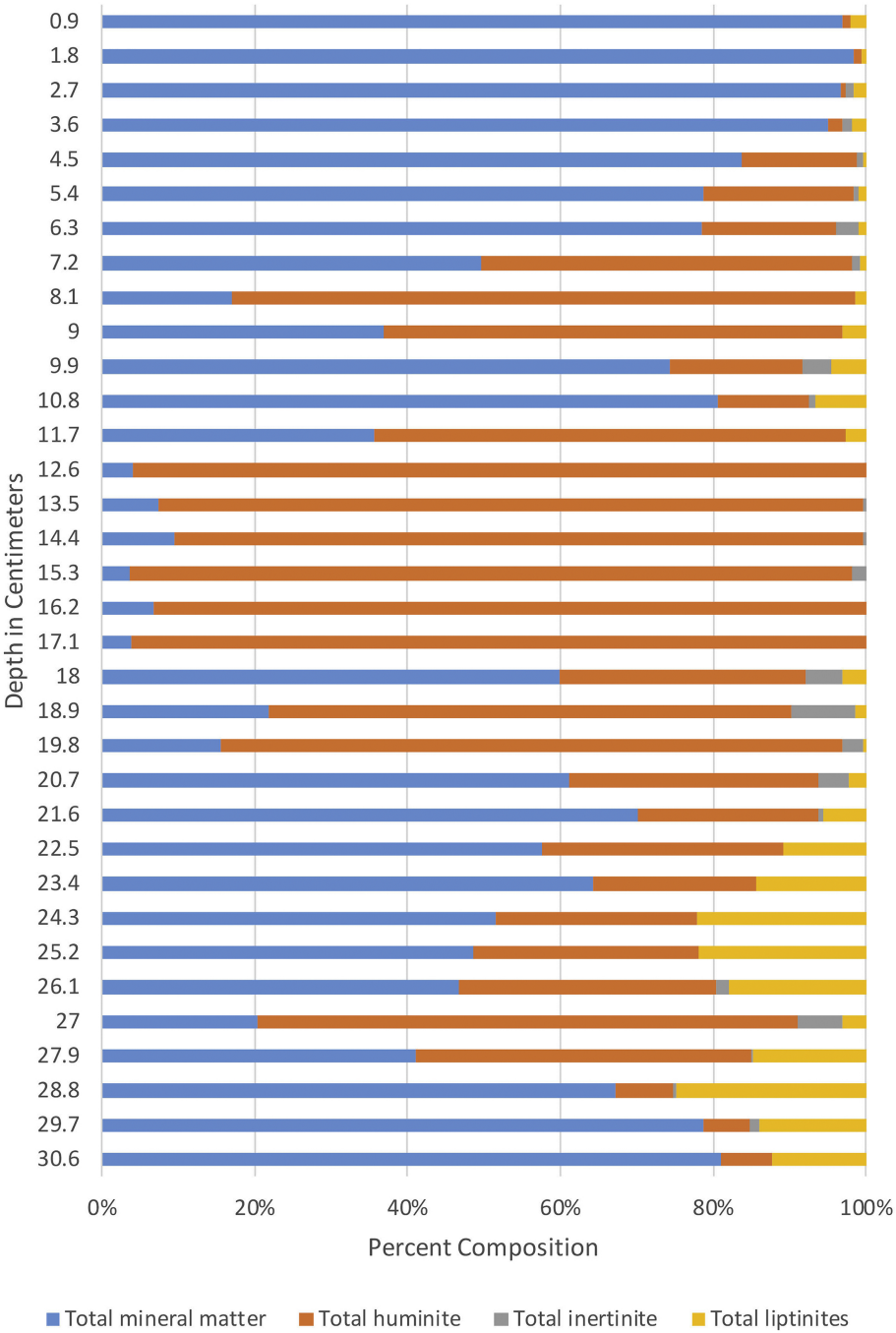
0.9
1.8
2.7
3.6
4.5
5.4
6.3
7.2
8.1
9
9.9
10.8
11.7
12.6
13.5
14.4
15.3
16.2
17.1
18
18.9
19.8
20.7
21.6
22.5
23.4
24.3
25.2
26.1
27
27.9
28.8
29.7
30.6
Depth in Centimeters
0%
20%
40%
60%
80%
100%
Percent Composition
Total mineral matter
Total huminite
Total inertinite
Total liptinites

Figure 7

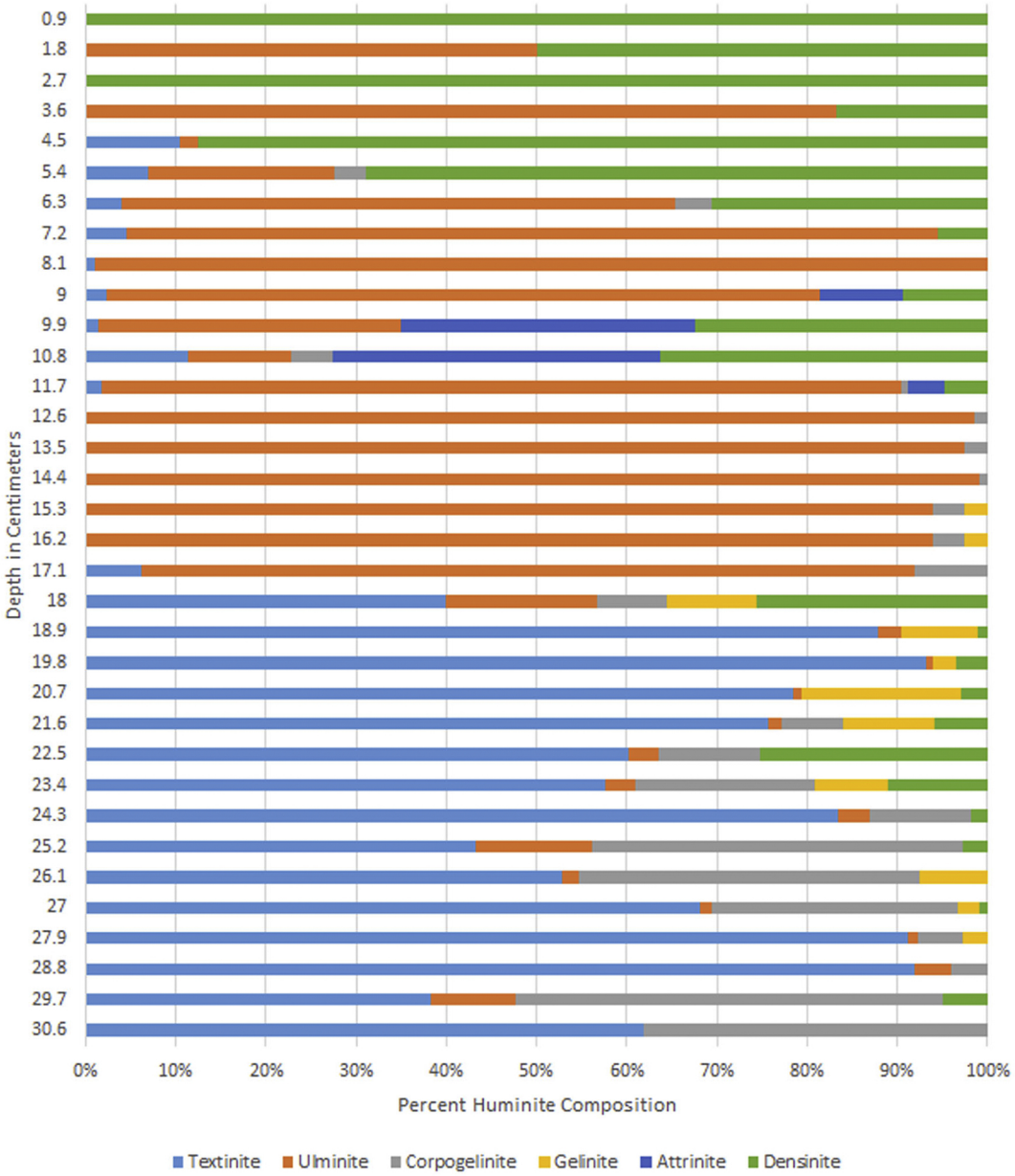
0.9
1.8
2.7
3.6
4.5
5.4
6.3
7.2
8.1
9
9.9
10.8
11.7
12.6
13.5
14.4
15.3
16.2
17.1
18
18.9
19.8
20.7
21.6
22.5
23.4
24.3
25.2
26.1
27
27.9
28.8
29.7
30.6
Depth in Centimeters
0%
10%
20%
30%
40%
50%
60%
70%
80%
90%
100%
Percent Huminite Composition
Textinite
Ulminite
Corpogelinite
Gelinite
Attrinite
Densinite

Figure 8

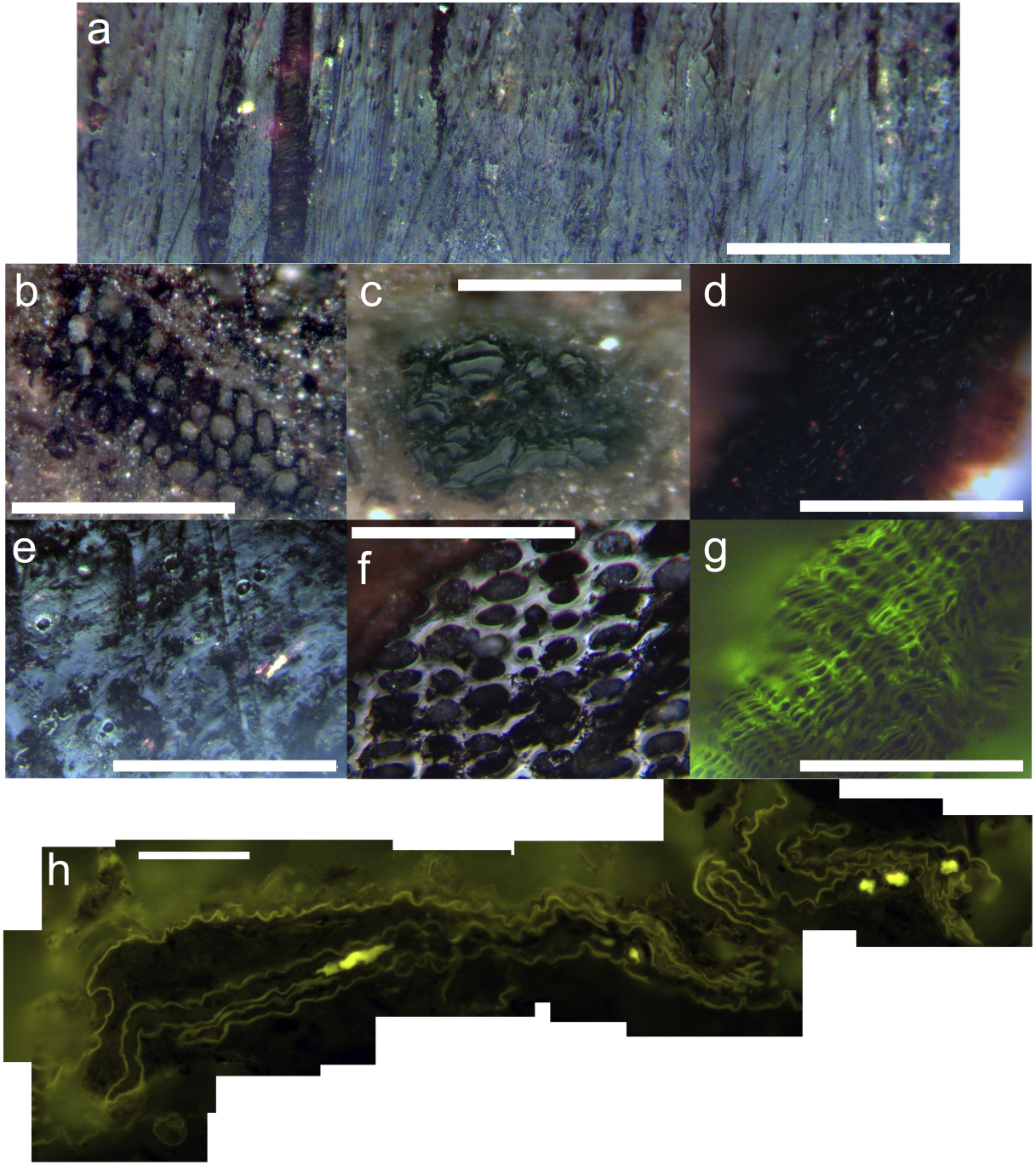

Figure 9

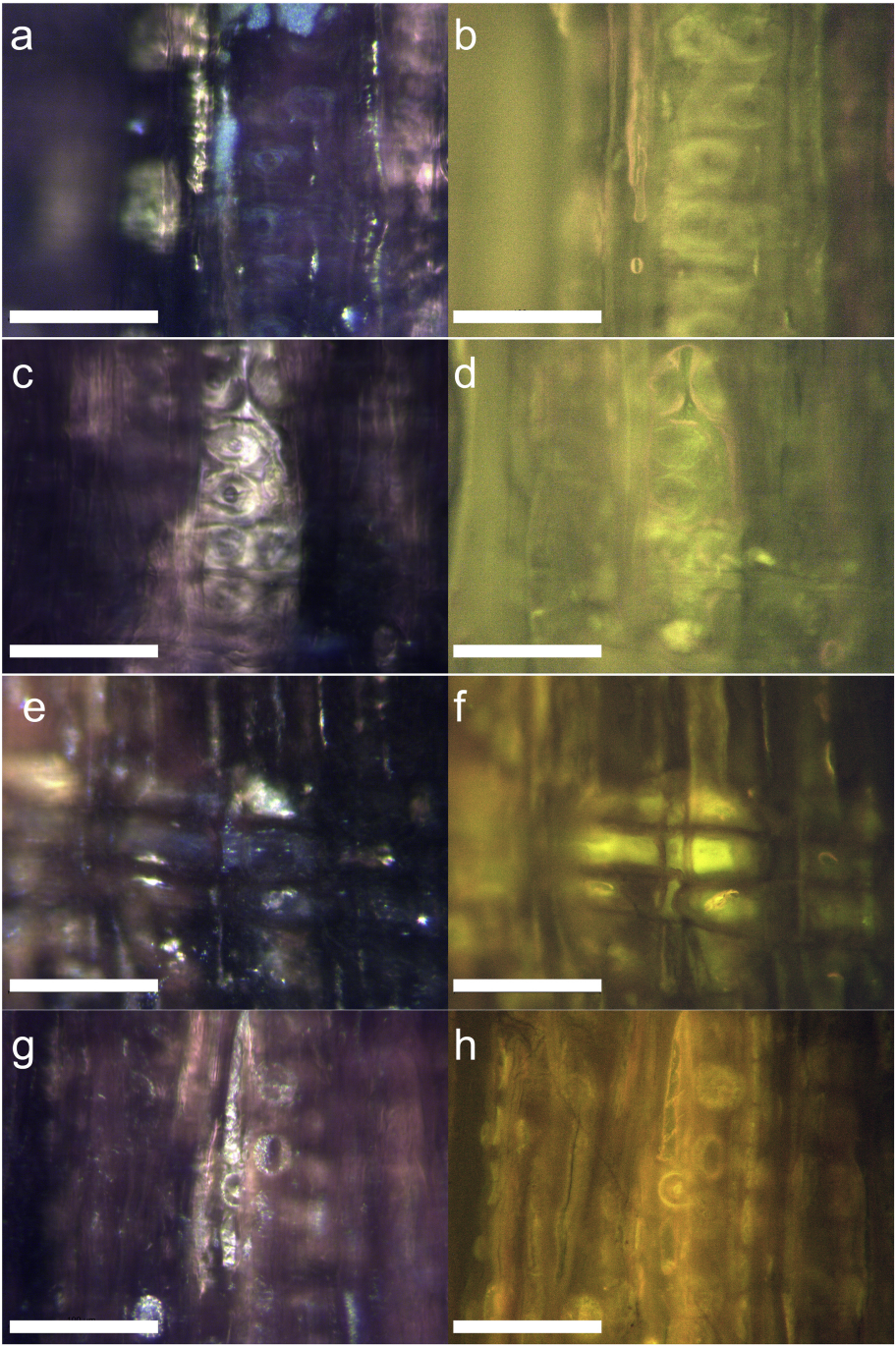

Figure 10

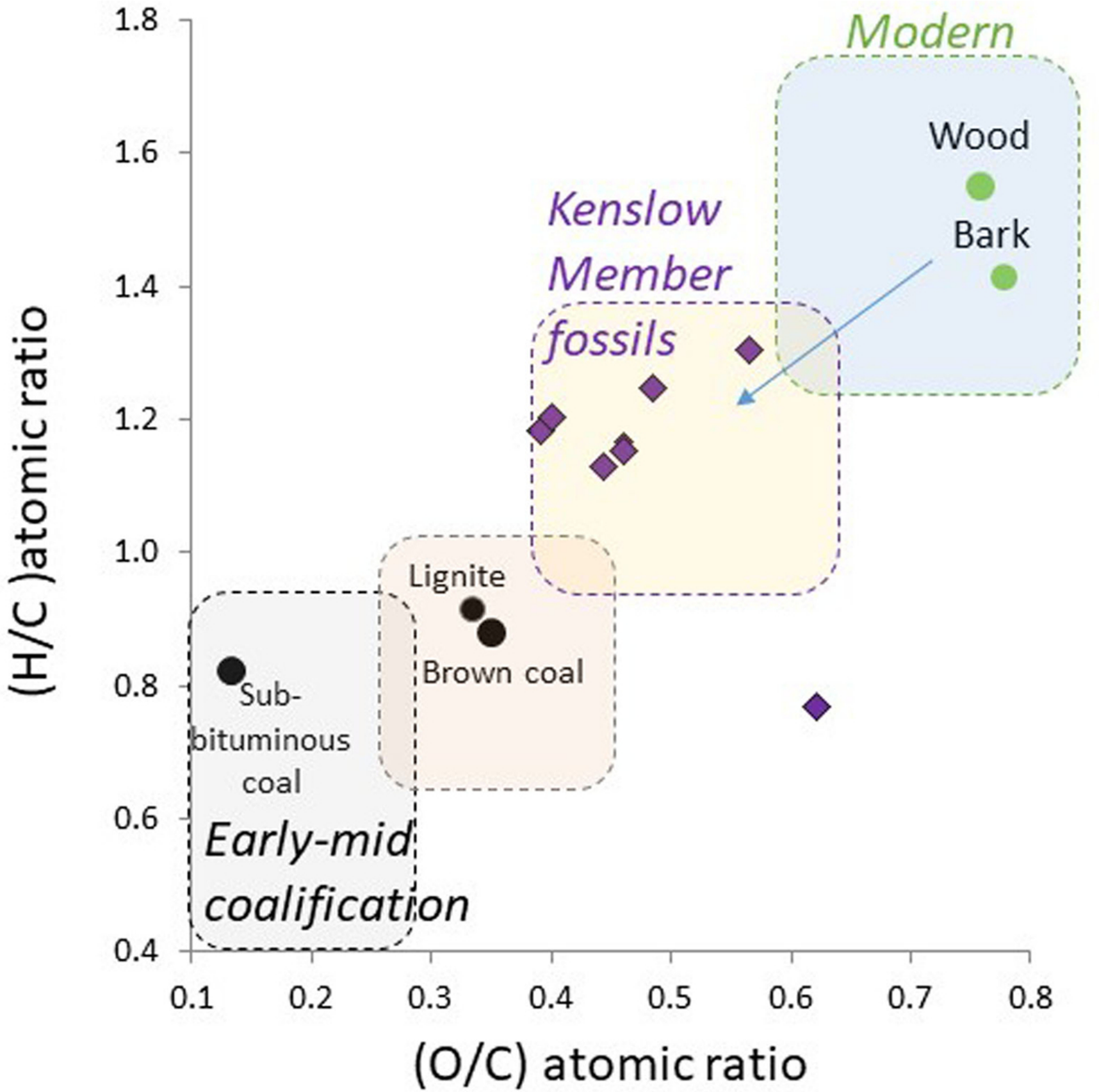
Modern
Wood
Bark
Kenslow Member fossils
Lignite
Brown coal
Sub-bituminous coal
Early-mid coalification
(H/C)atomic ratio
(O/C) atomic ratio
1.8
1.6
1.4
1.2
1.0
0.8
0.6
0.4
0.1
0.2
0.3
0.4
0.5
0.6
0.7
0.8

Figure 11